METHODS OF
Experimental Physics

VOLUME 22

SOLID STATE PHYSICS

Surfaces

7. HIGH-FIELD TECHNIQUES

By J. A. Panitz

Surface Science Division
Sandia National Laboratories
Albuquerque, New Mexico

"It seems as if the evasive atoms still hide from the curious eye of the casual sightseer and reveal themselves accordingly only to the serious researcher. . . ."[1]

7.1. Field-Electron-Emission Microscopy

It has been noted that "in the absence of lenses, illuminating devices, and automatic controls, a field-emission microscope is less of an apparatus and more of a direct aid to the eye and brain."[2] Perhaps for this reason field-emission microscopy made possible a direct observation of adsorption, desorption, and diffusion phenomena on atomically clean, single crystal metal surfaces by 1940, more than two decades before modern techniques of surface analysis became routinely available.

The foundation for field-electron-emission microscopy was established in the early 1900s with the discovery that an electron current could be measured between two room-temperature electrodes in high vacuum whenever a critical electric field strength was established between them.[3-6] In 1928 Eyring *et al.*[7] performed a classic experiment, which used sharply pointed cathodes of tungsten, nickel, and platinum placed opposite a planar tungsten anode. They found that the logarithm of the electron current striking the anode depended linearly on the reciprocal of the cathode potential. A sharply pointed cathode (or "tip") produced the same current as a dull tip, but at a lower voltage. This suggested that the electron emission process depended upon the electric field strength generated at the tip surface. In

[1] E. W. Müller, *Science (Washington, D.C.)* **149,** 591 (1965).
[2] T. G. Rochow and E. G. Rochow, "An Introduction to Microscopy by Means of Light, Electrons, X-Rays, or Ultrasound," p. 302. Plenum, New York, 1978.
[3] G. M. Hobbs, *Philos. Mag.* **10,** 17 (1905).
[4] R. A. Millikan and Shackelford, *Phys. Rev.* **12,** 167 (1918).
[5] R. A. Millikan and Shackelford, *Phys. Rev.* **15,** 239 (1920).
[6] R. A. Millikan and C. F. Eyring, *Phys. Rev.* **27,** 51 (1926).
[7] C. F. Eyring, S. Mackeown, and R. A. Millikan, *Phys. Rev.* **31,** 900 (1928).

METHODS OF EXPERIMENTAL PHYSICS, VOL. 22

ISBN 0-12-475964-5

order to estimate the field strength at the tip, Laplace's equation was solved using a geometry chosen to approximate the actual configuration of the electrodes. A family of equipotential contours was generated. One was matched to the contour of the tip measured from an optical micrograph and one to the planar anode. From the calculation, the electric field strength at the tip surface was shown to be several volts per nanometer. The method is still in use today, having been refined by many investigators.[8-10]

Eyring *et al.* thermally annealed each emitter tip in order to clean its surface. They baked their vacuum chamber in order to achieve very low pressures and had the option of selecting one of many tips by using a magnetically coupled manipulator. If they had deposited a fluorescent screen onto their tungsten anode, the modern field-electron-emission microscope would have been developed almost a decade earlier.

Although experimental evidence for field emission of electrons was well documented by 1928, theoretical predictions of the measured current–voltage characteristics were not particularly successful.[11,12] Until 1928, field emission was seen as a purely classical process in which electrons were thermally activated over a field-reduced energy barrier.[13] This model did not correctly predict the empirical relation[14] between the field emission current I and the voltage V applied to the tip

$$I = C \exp(-b/V), \tag{7.1.1}$$

where C and b are constants. A quantum mechanical treatment of the emission process was required in order to explain the empirical result.[15-17]

7.1.1. The Fowler–Nordheim Equation

In order for an electron to escape from a metal it must acquire sufficient energy to overcome the potential barrier at the surface presented by the work function Φ. Classically, the electron must be activated over the work function barrier. However, in the presence of a sufficiently large electric field the barrier will be distorted. In this case the probability for electron tunneling directly through the barrier will become significant as depicted in Fig. 1.

[8] J. A. Becker, *Bell Syst. Tech. J.* **30**, 907 (1951).
[9] W. P. Dyke, J. K. Trolin, W. W. Dolan, and G. J. Barnes, *J. Appl. Phys.* **24**, 570 (1953).
[10] M. Drechsler and E. Henkel, *Z. Angew. Phys.* **6**, 341 (1954).
[11] O. W. Richardson, *Proc. R. Soc. London, Ser. A* **117**, 719 (1928).
[12] J. M. Houston, *Z. Phys.* **47**, 33 (1928).
[13] W. Schottky, *Z. Phys.* **14**, 63 (1923).
[14] C. C. Lauritsen and R. A. Millikan, *Proc. Natl. Acad. Sci. U.S.A.* **14**, 45 (1928).
[15] R. H. Fowler and L. W. Nordheim, *Proc. R. Soc. London, Ser. A* **119**, 173 (1928).
[16] L. W. Nordheim, *Proc. R. Soc. London, Ser. A* **121**, 626 (1928).
[17] T. E. Stern, B. S. Gossling, and R. H. Fowler, *Proc. R. Soc. London, Ser. A* **124**, 699 (1929).

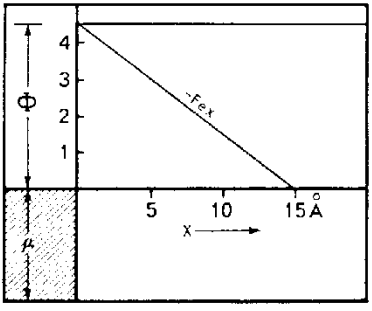

FIG. 1. A schematic energy diagram showing the work function barrier (here, equal to 4.5 eV) that an electron must overcome in order to escape from a metal surface. An applied electric field F distorts the barrier. This increases the probability of electron tunneling.

Field emission of electrons at low temperatures (in which direct thermal activation over the barrier can be neglected) is a direct manifestation of quantum mechanical tunneling, and as such has no classical analog. In fact, the success of the Fowler–Nordheim theory in predicting the current–voltage characteristic of field-emitted electrons was an early confirmation of the newly developed quantum theory of matter.

The field strength required for tunneling can be estimated from the Heisenberg uncertainty principle, as suggested by Gomer.[18] Appreciable tunneling will occur only when the uncertainty in the position of the electron becomes comparable to the width of the barrier Φ/Fe (see Fig. 1). If the uncertainty in the kinetic energy of the electron is taken to be of the order of the barrier height Φ, then

$$\Delta x\, \Delta p = (\Phi/Fe)(2m\Phi)^{1/2} \approx \hbar/2 \tag{7.1.2}$$

or

$$F \approx (8m\Phi^3/\hbar^2 e^2)^{1/2} \approx 10^8 \quad \text{V cm}^{-1}. \tag{7.1.3}$$

The field strength predicted by Eq. (7.1.3) is about an order of magnitude larger than required experimentally to detect a field emission current. The problem is the simplified triangular barrier of Fig. 1. It does not include the contribution of the coulombic attraction of the electron to its image charge in the metal $-e^2/4x$. Including the image potential will change the shape of the barrier as depicted in Fig. 2. The image potential is a classical concept. Strictly speaking, it must be inaccurate, at least for distances close to the surface where electron exchange and correlation effects are significant. However, it must be a reasonable approximation to the actual potential because

[18] R. Gomer, "Field Emission and Field Ionization." Harvard Univ. Press, Cambridge, Massachusetts, 1961.

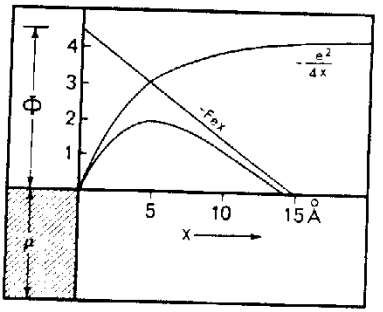

FIG. 2. A schematic energy diagram showing the shape of the potential barrier that results from applying an external field F to a metal if the classical coulombic image potential of the electron in the metal $-e^2/4x$ is included.

its use in the Fowler–Nordheim theory results in an accurate prediction of the current–voltage characteristic of field-emitted electrons.

In addition to the assumption of a classical image potential, the Fowler–Nordheim theory makes several other simplifying assumptions. These include

(1) the assumption that the tip behaves as though it were a simple, one-dimensional, free-electron-like metal, subject to Fermi–Dirac statistics at $T = 0$;

(2) the assumption that the tip surface can be approximated as a smooth, infinite plane (surface morphology is allowed provided that all features are much smaller than the width of the potential barrier); and

(3) the assumption that the work function Φ is uniform and isotropic over the tip surface.

Under these assumptions, if the barrier-penetration probability is calculated from the WKB approximation and multiplied by the arrival rate of electrons at the barrier, the result (in amperes per square centimeter) is the Fowler–Nordheim equation:

$$J = I/A = (1.54 \times 10^{-6}) \exp[-(6.83 \times 10^{7}) e^{3/2}\Phi^{3/2} f(y)/F][F^2/e\Phi t^2(y)], \tag{7.1.4}$$

where A is the emitting area, $t(y)$ and $f(y)$ are tabulated functions[19,20] of $y = (eF)^{1/2}/\Phi$, and the electric field strength is given by

$$F = V/KR. \tag{7.1.5}$$

[19] R. H. Good and E. W. Müller, in "Handbuch der Physik" (S. Flügge, ed.), Vol. 21, p. 176. Springer-Verlag, Berlin, and New York, 1956.

[20] A. G. J. Van Oostrom, *Philips Res. Rep., Suppl.* No. 1, p. 102 (1966).

For an isolated sphere in space $K = 1$. For actual tip geometries $3 \leq K \leq 6$.[21]

Equation (7.1.4) is of the form

$$I/V^2 = a \exp(-b\Phi^{3/2}/V).$$

If the logarithm of I/V^2 is plotted against $1/V$, a straight line is obtained. From the Fowler–Nordheim equation, the slope of this line is found to be

$$S = -b\Phi^{3/2} = 6.8 \times 10^7 e^{3/2}\Phi^{3/2} f(y)KR. \tag{7.1.6}$$

Assuming that the tip radius is known from a micrograph of the tip profile, and $K \approx 5$, the average work function of the emitter Φ can be obtained. On the other hand, if the average work function of the tip is known, KR can be directly determined.

7.1.2. The Field-Electron-Emission Microscope

In 1936 Johnson and Shockley[22] introduced the first microscope that used field-emitted electrons to form an image. It employed a cylindrical geometry in which a long thin wire served as the field emission cathode (see Fig. 3). The wire was stretched along the axis of a cylindrical glass envelope whose inside surface was covered with a transparent anode at ground potential. The anode was coated with a material that fluoresced under electron bombardment. By applying several thousand volts to the cathode, field emission was initiated. The resulting electrons were accelerated to the fluorescent screen where they

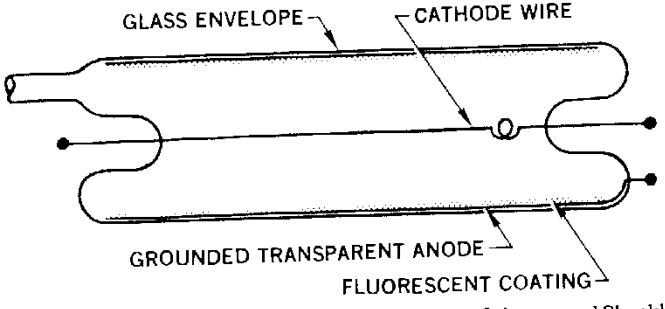

FIG. 3. A cylindrical field emission microscope developed by Johnson and Shockley in 1936. A fine-wire cathode is biased with respect to a fluorescent screen deposited on a transparent conductive anode that covers the inside diameter of an evacuated glass envelope. Axial magnification is unity. Radial magnification is determined by the ratio of wire diameter to screen diameter and is limited in practice to ~2000. The resolution of the microscope is usually worse than 10 nm.

[21] W. P. Dyke and W. W. Dolan, *Adv. Electron. Electron Phys.* **8**, 89 (1956).
[22] R. P. Johnson and W. Shockley, *Phys. Rev.* **49**, 436 (1936).

produced a pattern characteristic of the condition of the wire surface. By electrically heating the wire to a high temperature, the emission pattern became well defined and stable. The effect was correctly interpreted as an example of surface cleaning by thermal desorption of contaminant species.[22]

Crystal growth could be observed by uniformly coating the cathode wire with cesium. Cesium produces an almost contrastless emission pattern. As the temperature of the wire was increased to several thousand degrees Kelvin, the pattern changed in a way that suggested that individual crystallites were developing. Their size and shape could be studied as a function of wire temperature by observing the room-temperature emission pattern after heat treatment. Thermal activation of thoriated tungsten[23] and molybdenum[24,25] was studied in a similar manner. The results helped to clarify the nature of the activation process, which was commercially important to the developing vacuum tube industry.

The magnification and resolution of the cylindrical microscope are different in the axial and radial directions because of its nonspherical symmetry. As a result, the field emission image is distorted, making image interpretation difficult. In order to correct the problem, Erwin Müller[26,27] designed a spherically symmetric field-electron-emission microscope (or FEEM) that is still used today. Müller's microscope, introduced in 1936, was virtually identical to the design of Erying and co-workers. Field-emitted electrons were projected from a tip to an anode covered with a fluorescent material. The apparatus is shown schematically in Fig. 4. A fine wire is formed into a triangular loop with the protruding end etched to a needlelike point. One side of the loop bridges two supporting electrodes. The electrodes can be outgassed by passing an electric current through them. If the current is suddenly increased, the bridge will "burn out," and the tip assembly can be independently outgassed. By controlling the current, the tip can be thermally annealed at an elevated temperature. The conductive anode is formed by vapor depositing tin oxide onto the glass envelope of the microscope. The anode is coated with zinc oxide or Willemite ($ZnSiO_4$: Mn) in order to make the emission pattern visible.

Side arms contain sublimation sources aimed at the tip, and a barium getter is used to achieve ultrahigh-vacuum conditions. The pressure in the microscope body can be deduced from the change in the appearance of the field emission pattern with time. As residual gas contaminants are adsorbed onto the tip apex, they will become visible in the emission pattern. If a

[23] A. J. Ahearn and J. A. Becker, *Phys. Rev.* **49**, 879 (1936).
[24] E. Bruche and H. Mahl, *Z. Tech. Phys.* **16**, 623 (1935).
[25] E. Bruche and H. Mahl, *Z. Tech. Phys.* **17**, 81 (1936).
[26] E. W. Müller, *Z. Phys.* **37**, 838 (1936); **102**, 734 (1936).
[27] E. W. Müller, *Z. Tech. Phys.* **17**, 412 (1936).

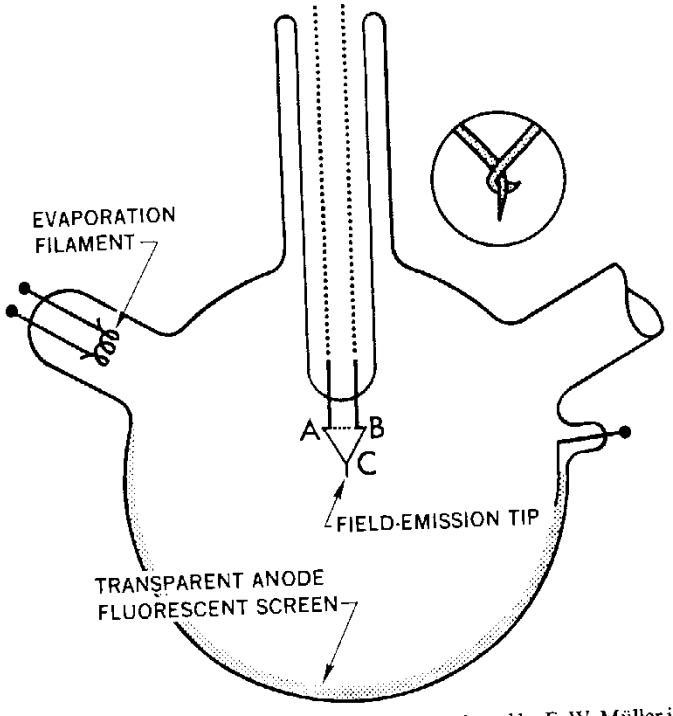

FIG. 4. A point-projection field emission microscope developed by E. W. Müller in 1936 and in use today. Magnifications of $\sim 10^6$ at a resolution of ~ 20 nm are routinely achieved. A flat fluorescent screen is usually used in order to achieve better quality photographs of the field emission pattern. The insert shows the tip assembly (C) in more detail.

sticking probability of unity is assumed, the number of adsorption events per unit time measured from the emission pattern is directly proportional to the pressure in the microscope. Since all adsorbates do not cause visible changes in an emission pattern, the method is not entirely reliable. However, it can be more accurate than a hot-filament pressure gauge, particularly at very low pressures, for which outgassing, selective adsorption, or x-ray production may present a problem.

The size of a tip apex is usually smaller than the size of the individual crystallites in most polycrystalline materials. This means that a tip etched from polycrystalline material will usually be formed from a single perfect crystal. (Occasionally, a tip will be etched from two or more single crystallites of the polycrystalline material separated by well-defined grain boundaries.) The etching process exposes at the surface of the tip apex many different crystal planes of low and high Miller indices, smoothly joined into an ap-

proximately hemispherical contour. A typical tip profile is shown in the transmission electron micrograph of Fig. 5. Individual crystal planes may have different packing densities of atoms resulting in inherently different charge distributions. As a result, the work function of a clean tip will vary over its surface depending on local crystallography. The field emission image will reflect the local crystallography of the surface because the probability of field-emitting an electron will depend on the local work function. Since surface adsorbates will tend to change the local work function, they can often be seen in the field emission pattern as a localized contrast variation. The simplicity of the FEEM technique allowed Müller[28] to study adsorption and desorption phenomena on clean metal surfaces in ultrahigh vacuum, as early as 1937.

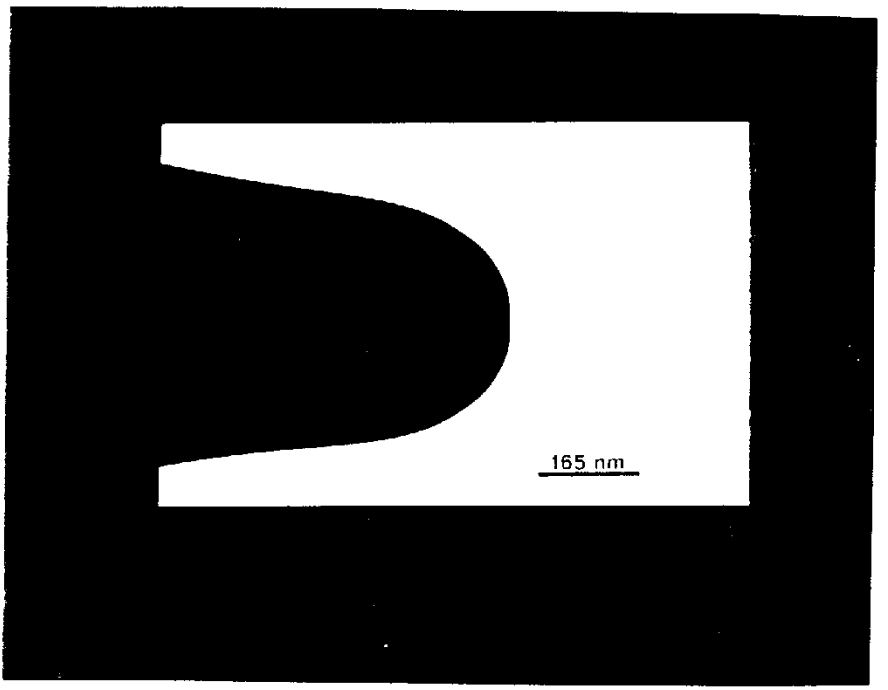

FIG. 5. A thermally annealed field-emitter tip viewed in profile in the transmission electron microscope. The tip was prepared by electrochemical polishing of a fine wire (typically 0.1 mm in diameter). Following the electropolish, the tip was heated in vacuum close to its melting point.

[27a] J. A. Panitz, *J. Phys. E* **15**, 1281 (1982).
[28] E. W. Müller, *Z. Phys.* **106**, 132, 541 (1937).

7.1.3. The Magnification of a Point-Projection Microscope

A microscope that magnifies by projecting a charged species from a highly curved surface to a detector is called a "point-projection" microscope. The FEEM is such a device. Because lenses are not used, the magnification M of the image is determined purely by geometric considerations (see Fig. 6). If a tip of radius R is placed a distance D from a fluorescent screen, the magnification will be

$$M = S/s_0 = (D + \beta R)/\beta R \simeq D/\beta R, \tag{7.1.7}$$

where $\beta = 1.5$ is an "image compression factor." It describes the deviation from pure radial projection ($\beta = 1$) caused by the presence of the tip wire and its supporting assembly. Since the tip radius is typically less than a few hundred nanometers, a very high magnification is easy to achieve.

It is important to emphasize that the magnification of a point-projection microscope relies only on geometric considerations. Unlike other microscopes a probing beam of charged particles is not required. Lenses are unnecessary and the substrate cannot move relative to a probing species. As a result, image aberrations are minimal, and external vibrations will not be magnified. This means that a useful magnification of several million times can be achieved in practice.

The radius of a tip can be accurately determined by viewing the tip in

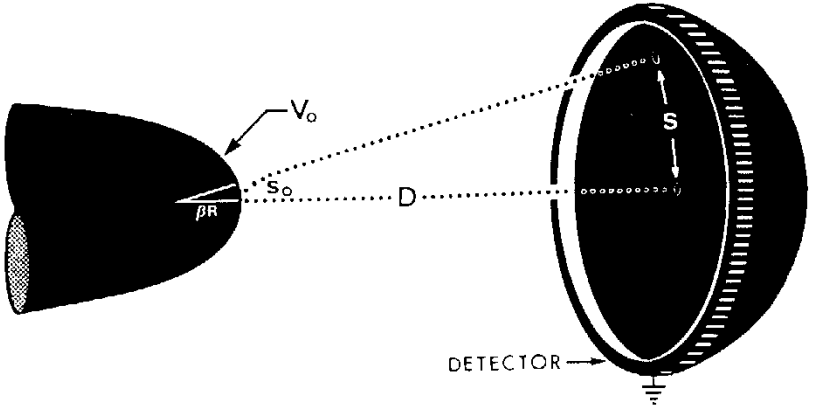

FIG. 6. A schematic representation of the geometric process used to obtain magnification in a point-projection microscope. A specimen top is biased to a positive potential V_0. Charged particles formed in the vicinity of the tip apex are accelerated almost radially into space. If the trajectories from the tip are projected backward, they will tend to intersect within the tip at a distance βR from its surface. βR can be treated as an effective tip radius. R is the measured radius of the tip and β is an "image compression" factor. For an isolated sphere in space $\beta = 1.0$. (From Panitz.[27a] Copyright 1982 The Institute of Physics.)

profile in the transmission electron microscope (Fig. 5). Since the tip-to-detector distance can also be accurately measured, the uncertainty in the magnification of a point-projection microscope will be determined by the uncertainty in the image compression factor. Unfortunately, the image compression factor is tip dependent. Although β can be determined for each tip from a trajectory calculation employing an idealized tip of comparable shape and dimensions,[29] the procedure is only an approximation. Furthermore, the actual magnification of an image will vary locally across the image because of local variations in the radius of curvature of the tip. Although this is generally a small effect, the uncertainty in β means that the magnification of an FEEM image is only known to within thirty or forty percent.

7.1.4. The Resolution of a Point-Projection Microscope

The resolution of a point-projection microscope is limited by the velocity component of the charged species parallel to the tip surface as it accelerates into space. Consider two adjacent species at the surface of the tip apex. If T is the time that it takes for each species to travel from the tip to the fluorescent screen, and v_T is their transverse velocity, then the species will have separated by a distance $= 2v_T T$ when they reach the screen. The resolution of the microscope cannot be better than this distance δ projected back onto the tip surface, where

$$\delta = 2v_T T\beta R/D \tag{7.1.8}$$

and $D/\beta R$ is the magnification. Since a charged particle acquires its full kinetic energy very close to the tip, its travel time is approximately equal to the time required for it to drift over the tip-to-screen distance with maximum velocity v_R. In other words

$$T \approx D/v_R = D(m/2neV)^{1/2}, \tag{7.1.9}$$

where m/ne is the mass-to-charge ratio of the species, and V is the potential applied to the tip. If Eqs. (7.1.3) and (7.1.4) are combined, the resolution becomes

$$\delta = 2\beta R v_T/v_R = v_T(2m\beta^2R^2/neV)^{1/2}. \tag{7.1.10}$$

During field emission, there are two contributions to v_T. The first is just the average transverse velocity that the electrons possess as they leave the metal surface, essentially equal to their Fermi velocity. The second is caused by their finite de Broglie wavelength. Consider an electron localized to a region of the tip surface Δx. From the Heisenberg uncertainty principle, its corre-

[29] L. W. Swanson, *Proc. Int. Field-Emiss. Symp., 29th,* Goteborg, Sweden, p. 101. (1982). Edited by H. Nordén and H. O. Andren (Almquist and Wiksell, International, Stockholm.).

sponding momentum parallel to the tip surface will be uncertain by $\hbar/2\,\Delta x$. Consequently, the uncertainty in the average transverse velocity of field-emitted electrons due to diffraction will be

$$v_D = \hbar/2m\,\Delta x. \tag{7.1.11}$$

Müller[30] combined both contributions quadratically to obtain a resolution of about twenty angstroms, in agreement with experiment. Rose,[31] and later Brodie,[32] argued that, under very special conditions, atomic resolution ($\delta \approx$ 0.4 nm) might also be possible.

7.1.5. Adsorption Studies Using the FEEM

If the average work function of the clean tip is known, the change in work function corresponding to adsorption on the surface can be determined. Experimentally, one measures the ratio of the Fowler–Nordheim slope before and after adsorption and assumes that KR remains constant.[18] From Eq. (7.1.11):

$$\Phi_a = (S_a/S_c)^{3/2}(f_c/f_a)^{2/3}\Phi_c, \tag{7.1.12}$$

where the subscript a means *after adsorption*, and the subscript c denotes the clean tip surface *prior to adsorption*. Since $(f_c/f_a)^{2/3} \approx 1$, the relative change in the average work function due to adsorption can be determined. The accuracy of Eq. (7.1.12) depends upon the assumption that the regions of the emitter that contribute most strongly to emission prior to adsorption will contribute most strongly after adsorption. Since this is not always true, it is best to measure the work function change of small regions of the emitter such as single crystal planes. Although an apertured photomultiplier can be used to examine selected areas of the field emission pattern, it is difficult to eliminate contributions due to light scattered from high-emission areas of the tip. Therefore, a "probe hole" technique is usually used.[32–36]

In probe-hole field emission microscopy, the tip is manipulated so that the field emission image can be shifted with respect to a small aperture (or probe hole) in the fluorescent screen. A Faraday collector or electron multiplier is placed behind the probe hole in order to measure the field emission current. In principle, if the aperture is made much smaller than the area of the region being examined, a reasonably accurate measurement of local work function

[30] E. W. Müller, *Ergeb. Exakten Naturwiss.* **27**, 290 (1953).
[31] D. J. Rose, *J. Appl. Phys.* **27**, 215 (1956).
[32] I. Brodie, *Surf. Sci.* **70**, 186 (1978).
[33] E. W. Müller, *Z. Phys.* **120**, 261, 270 (1943).
[34] W. M. H. Sachtler, *Angew. Chem.* **80**, 673 (1968).
[35] B. E. Nieuwenhuys and W. M. H. Sachtler, *Surf. Sci.* **34**, 317 (1973).
[36] M. Domke, G. Jahnig, and M. Drechsler, *Surf. Sci.* **42**, 389 (1974).

can be made. Of course, one is never certain that all electrons from adjacent regions of the emitter will be excluded from the measurement.

The probe-hole technique has made a major contribution to our understanding of the work function concept. If nitrogen is adsorbed onto macroscopic samples of polycrystalline tungsten, a large variation in the work function (0–0.12 eV) is observed with microscopic techniques.[37,38] Probe-hole field emission experiments[39,40] demonstrate that both the magnitude and the direction of the polarization (the sign of Φ) depend on the crystal plane under examination. Since macroscopic measurements average the work function over a large area of the specimen, the wide variation in work function measured for polycrystalline samples can be explained.

Although individual adsorbates cannot always be observed in an FEEM image, the local work function of the tip surface is very sensitive to their presence. As a result, the fractional coverage of an adsorbate on the tip is usually obtained indirectly from a change in work function on adsorption. As a first approximation, a dipole moment P can be associated with each adsorbed species.[18] In this case, the work function change due to adsorption can be written as

$$\Delta\Phi = CN_T P, \tag{7.1.13}$$

where N_T is the total number of adsorbed species, and C is a constant of proportionality. If the coverage θ is defined as the number of species adsorbed on the surface N_T divided by the number of sites available on the surface for adsorption N, then

$$\Delta\Phi = CNP\theta. \tag{7.1.14}$$

Although $C \approx 4\pi^3$, its actual value is not known, so that an absolute coverage cannot be obtained from Eq. (7.1.14). If the dipole moment associated with each adsorbate is independent of coverage, a relative coverage in terms of some maximum coverage θ_{max} can be obtained from Eq. (7.1.14), where

$$\theta_{max} = \Delta\Phi/\Delta\Phi_{max}. \tag{7.1.15}$$

Strictly speaking, Eq. (7.1.15) is valid only in small, localized regions of the surface where crystallographic variations in the dipole moment for each adsorbate can be neglected.

It should be apparent from the previous discussion that qualitative information concerning an adsorbate–substrate interaction is very easy to obtain

[37] M. P. Hill and B. A. Pethica, *J. Chem. Phys.* **38**, 567 (1963).
[38] C. M. Quinn and M. W. Roberts, *J. Chem. Phys.* **40**, 237 (1964).
[39] A. A. Holscher, *J. Chem. Phys.* **41**, 579 (1964).
[40] A. G. J. Van Oostrom, *J. Chem. Phys.* **47**, 761 (1967).

from the appearance of the field emission pattern and its current–voltage characteristic. Although relative values of work function and coverage can be easily obtained, absolute values are difficult or impossible to measure. Fortunately, there is another type of field emission measurement that can provide detailed information on the nature of the adsorbate–substrate interaction. The measurement involves a determination of the kinetic energy distribution of the electrons field-emitted from the tip. Intuitively, one would expect that the energy distribution would be sensitive to the electronic properties of a clean metal surface and reflect any modification of the tunneling process resulting from a change in surface charge distribution on adsorption.

7.1.6. Field Emission Energy Distributions

The energy distribution of field-emitted electrons was measured before 1940 by several investigators.[26,41,42] These measurements were constrained by poor energy resolution. In 1959 the first measurement of the true narrow half-width of the total energy distribution was made by Young.[43,44] Prior to Young's observations, it was assumed that the field emission energy distribution (FEED) measured only those electrons that had a component of velocity normal to the tip surface.[19,45] Actually, electrons having both perpendicular *and* transverse energy components to the emitter surface contribute to the measured current. It is experimentally impossible to distinguish between the two. Transverse momentum is quickly dominated by the forward momentum that an electron acquires in the radially diverging field above the emitter surface.[46]

Many devices have been constructed in order to measure the total energy distribution of field-emitted electrons. Most operate as retarding-potential analyzers.[20,44,47–50] A typical analyzer consists of three electrodes. The field-emitter tip held at potential V_T, is the first. The second consists of an apertured counter–electrode that acts as the anode. It is held at potential V_A. The third electrode is a collector located immediately behind the aperture in the anode. It is held at potential V_C. The retarding analyzers that appear in the

[41] J. E. Henderson and R. E. Badgley, *Phys. Rev.* **38,** 540 (1931).
[42] R. K. Dahlstrom, K. V. Mackenzie, and J. E. Henderson, *Phys. Rev.* **48,** 484 (1935).
[43] R. D. Young, *Phys. Rev.* **113,** 110 (1959).
[44] R. D. Young and E. W. Müller, *Phys. Rev.* **113,** 115 (1959).
[45] E. L. Murphy and R. H. Good, Jr., *Phys. Rev.* **102,** 1464 (1956).
[46] J. W. Gadzuk and E. W. Plummer, *Rev. Mod. Phys.* **45,** 487 (1973).
[47] L. W. Swanson and A. E. Bell, *Adv. Electron. Electron Phys.* **32,** 193 (1973).
[48] R. D. B. Whitcutt and B. H. Blott, *Phys. Rev. Lett.* **23,** 639 (1969).
[49] E. W. Plummer and R. D. Young, *Phys. Rev. B* **1,** 2088 (1970).
[50] C. Lea and R. Gomer, *J. Chem. Phys.* **54,** 3349 (1971).

literature differ primarily in their geometry, the method that they use to manipulate a selected region of the field emission image over the anode aperture, and the method used to focus the electrons onto the collector. In all cases, the field strength required for electron emission is established by the potential difference that is applied between the emitter tip cathode and the anode ($V_A - V_T$). Only electrons that have sufficient kinetic energy to overcome the retarding potential difference established between the collector and the tip ($V_C - V_T$) will be measured. The variation in the collector current as a function of retarding potential is the integral of the total energy distribution of the field-emitted electrons. Energy distributions are obtained by graphical or electronic differentiation.

A typical retarding-potential analyzer has an energy resolution of $\Delta E/E \approx 30$ mV, and a signal-to-noise ratio of $\Delta I/I \approx 0.01$. To improve performance, a spherical electrostatic deflection analyzer was developed by Kuyatt and Plummer.[51] A computer-optimized lens system maximized the collected current and provided an energy resolution of ~20 mV at a signal-to-noise ratio of about 1000 : 1.

A clean tip surface characteristically produces a single peak in the energy distribution of field-emitted electrons. Swanson and Crouser were the first to observe two peaks in the energy distribution of electrons emitted from the (100) plane of tungsten.[47] The height of the peak (at 0.37 eV) was shown to be a sensitive function of the cleanliness of the surface. This feature (which has become known as the *Swanson hump*) is easily attenuated by the adsorption of a partial monolayer of CO, H_2, N_2, O_2, or even Kr or Xe.[49,50,52,53] Conflicting theories of the origin of the Swanson hump appear in the literature. Gadzuk and Plummer[46] appear to have demonstrated that the structure is due to a surface state in the $\langle 100 \rangle$ spin–orbit-split gap of tungsten. Figure 7 shows a comparison of Gadzuk's calculation with the measured energy distribution from the (100) plane of tungsten.[54] The energy scale in Fig. 7 has been shifted so that the zero of energy lies at the Fermi energy E_F.

Field-electron energy distribution instrumentation and the interpretation of FEED data in terms of band structure, surface states, and adsorption have been discussed in several excellent reviews.[45,55,56] It is clear that FEED data is sensitive to such phenomena. However, it is not always a simple matter to

[51] C. E. Kuyatt and E. W. Plummer, *Rev. Sci. Instrum.* **43**, 108 (1972).
[52] E. W. Plummer and J. W. Gadzuk, *Phys. Rev. Lett.* **25**, 1493 (1970).
[53] E. W. Plummer and A. E. Bell, *J. Vac. Sci. Technol.* **9**, 583 (1972).
[54] J. W. Gadzuk, *J. Vac. Sci. Technol.* **9**, 591 (1972).
[55] J. W. Gadzuk and E. W. Plummer, *Solid State Surf. Sci.* **3**, 165 (1973).
[56] L. W. Swanson and A. E. Bell, *Adv. Electron. Electron Phys.* **32**, 193 (1973).

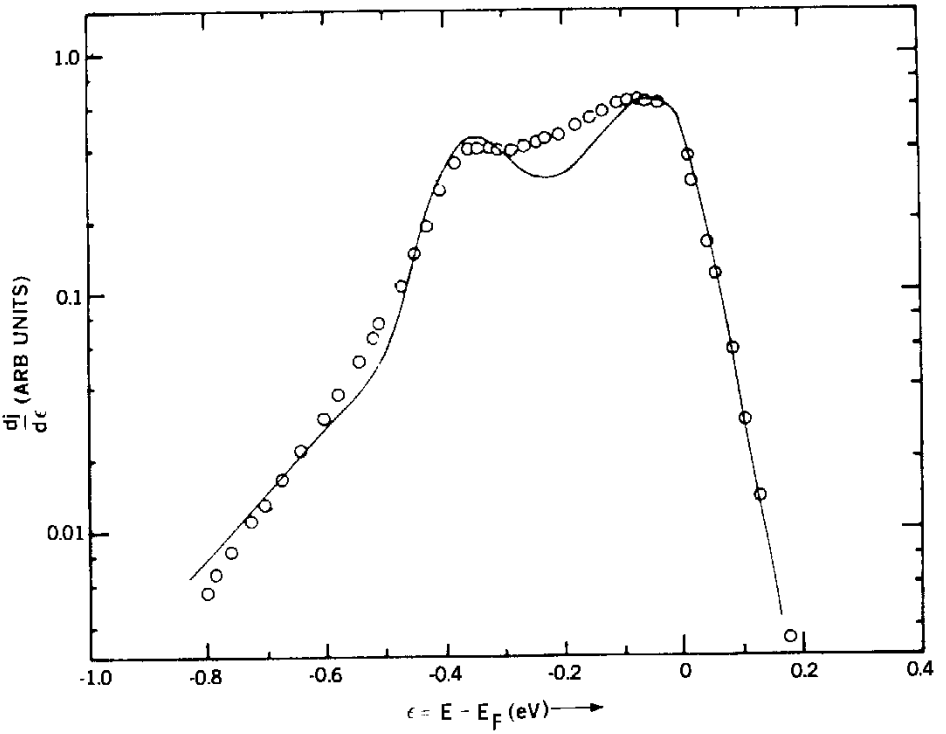

FIG. 7. A comparison of the experimental (O), and theoretical (–) total energy distribution of field-emitted electrons from the (100) plane of tungsten. Experimental parameters are $\Phi = 4.65$ eV, $F = 0.368$ V Å^{-1}, $T = 300$ K. [Figure courtesy of J. W. Gadzuk (The National Bureau of Standards, Washington, D.C.).]

interpret structure in the experimental energy distributions in terms of such phenomena.[46] In addition, it is difficult to probe very far from the Fermi energy, which limits the utility of this powerful technique.

7.2. Applications of Field-Electron-Emission Microscopy

7.2.1. Surface Diffusion

One of the most direct applications of field emission microscopy is the study of adsorbate diffusion on clean metal surfaces as a function of surface coverage. The usual method relies on observing changes in the intensity of a field emission pattern as an adsorbate diffuses over the surface at some well-defined temperature T. To minimize the possibility of the electric field

affecting the measurement, diffusion is usually initiated at elevated temperatures in the absence of a field. The field emission pattern after diffusion is observed in the presence of the field but at a lower temperature for which surface diffusion is negligible. Since the resolution of the FEEM does not usually allow individual adsorbate motion to be observed, only the motion of an ensemble of adsorbates can be easily seen. Such diffusion is usually characterized by the movement of a sharp boundary, which delineates the adsorbate layer from the clean metal surface. From the observed movement of the boundary as a function of diffusion temperature and time, the diffusion coefficient and the activation energy for surface diffusion can be obtained.

One interesting system involves the diffusion of a mobile physisorbed layer on top of an immobile chemisorbed layer. Although such phenomena can be observed by cooling the emitter tip to below the multilayer condensation temperature of the adsorbate, it is preferable to cool the entire microscope in a cryostat. This technique, pioneered by Gomer,[18,57] ensures that all surfaces are held below the condensation temperature of the adsorbate. Since each molecule that arrives at a surface will be effectively removed from the gas phase, only those regions of the tip in a direct line of sight with the effusion source of the adsorbate will be covered.

Gomer *et al.*[58-60] demonstrated that three distinct types of diffusion could occur for hydrogen and oxygen on tungsten. The particular type of diffusion depended on the morphology of the surface. If more than a monolayer of adsorbate was deposited, uniform diffusion with a sharp boundary was observed below 20 K for hydrogen, and below 30 K for oxygen. Gomer[18] explained the observations by assuming that a mobile physisorbed layer was diffusing on top of an immobile chemisorbed layer. When the molecules in the physisorbed layer reached the edge of the chemisorbed layer, they "precipitated" onto the clean surface, where they chemisorbed, thereby extending the sharp boundary. Gomer characterized this type of diffusion by an average diffusion constant

$$D = \bar{x}^2/t, \tag{7.2.1}$$

where $\bar{x}$ is the average distance traversed by the boundary at time t. He calculated an activation energy for diffusion by assuming a diffusion coefficient of the form

$$D = A^2\nu \exp(-E_d/kT), \tag{7.2.2}$$

[57] R. Gomer and J. K. Hulm, *J. Am. Chem. Soc.* **75**, 4114 (1953).
[58] B. Halpern and R. Gomer, *J. Chem. Phys.* **51**, 3043 (1969).
[59] R. Gomer, R. Wortman, and R. Lundy, *J. Chem. Phys.* **26**, 1147 (1957); R. Wortman, R. Gomer, and R. Lundy, *J. Chem. Phys.* **27**, 1099 (1957).
[60] R. Gomer and J. K. Hulm, *J. Chem. Phys.* **27**, 1363 (1957).

where $\nu \approx 10^{12}$ s^{-1}, and $A \approx 0.3$ nm. Typical activation energies for diffusion ranged from 24.8 ± 1 kcal for O_2 on W(110) to 5.9 ± 1 kcal for H_2 on W(110).

For monolayer coverages a second type of diffusion was observed at temperatures above 180 K for hydrogen, and above 500 K for oxygen. This type of diffusion was characterized by a diffusion boundary that spread outward from the smooth close-packed (110) plane, advancing most rapidly along crystallographic zones characterized by an atomically smooth surface. Gomer reasoned that on the smooth regions of the tip, the activation energy for surface migration is high. However, upon reaching a rougher surface topography for which the activation energy for diffusion is lower, the adsorbate would become interstitially trapped.

At coverages much less than a monolayer, a third type of diffusion was observed. At very low coverages, the rate of diffusion is not limited by migration over the smooth (110)-like regions of surface but by the number and size of "trap" sites on the rougher adjacent regions of the surface. In this case, an activation energy of 30 ± 1.5 kcal was obtained for oxygen, whereas for hydrogen 9.6 to 16 ± 3 kcal was obtained.

Many other adsorption systems have been studied by using the field emission technique. These include O_2 on tungsten,[61] CO on tungsten,[62-64] CO_2 on tungsten,[65] and Kr, Xe, Ne, and Ar on tungsten and titanium.[66-68] At submonolayer coverages, inert gas diffusion is characterized by an immobile boundary with enhanced emission appearing on initially clean regions of the tip. Since chemisorption cannot occur, the first layer of inert gas must be physically adsorbed to the substrate. Enhanced emission suggests that the inert gas layer decreases the local work function of the substrate. Under conditions of multilayer adsorption, diffusion is observed to proceed in "waves" or steps. At high temperatures, thermal desorption of the multilayer appears in the field emission pattern as a series of almost concentric boundaries that shrink toward the center of the tip at different rates.[18] These observations suggest that the inert gas boundary can be characterized by a liquid-like flow of the adsorbate where line tension forces (the two-dimension analog of surface tension forces) predominate. The outermost layers appear to behave as two-dimensional anisotropic liquids in which evaporation of

[61] E. W. Müller, *Z. Elektrochem.* **59**, 372 (1955).
[62] G. Ehrlich, T. W. Hickmott, and F. G. Hudda, *J. Chem. Phys.* **28**, 506 (1958).
[63] R. Gomer, *J. Chem. Phys.* **28**, 168 (1958).
[64] R. Klein, *J. Chem. Phys.* **31**, 1306 (1959).
[65] D. O. Hayward and R. Gomer, *J. Chem. Phys.* **30**, 1617 (1959).
[66] R. Gomer, *J. Chem. Phys.* **29**, 441 (1958).
[67] R. Gomer, *J. Phys. Chem.* **63**, 468 (1959).
[68] G. Ehrlich and F. G. Hudda, *J. Chem. Phys.* **30**, 493 (1959).

adsorbate atoms is most probable at the layer edge, where binding is the weakest.[18]

Isosteric heats of adsorption can be determined from field emission measurements. By using a probe-hole technique, these can be measured as a function of local surface crystallography.[36] With some sophistication, the absolute coverage of an adsorbate can also be obtained. Gomer and coworkers[69,70] have measured the absolute coverages of CO and O_2 on tungsten (110), and the sticking coefficient of CO, O_2, and Xe on tungsten (110) and (100) by using a novel field emission detector and a calibrated effusion source.

It is clear that field emission microscopy can provide a unique view of the diffusion process on an atomic scale. However, the technique suffers from two major difficulties. Since visual observations can be made only if the adsorption process causes a change in image contrast, it may be difficult to obtain information on a particular diffusion process of interest. In addition, diffusion observed in one region of the emitter surface will generally occur only after an adsorbate has migrated over adjacent regions of the tip. Since the adsorbate may encounter a variety of different surface conditions before it diffuses into the region of interest, it is difficult to correlate a diffusion constant with a unique regional morphology. In an attempt to overcome these difficulties, Gomer[71] has suggested another measurement technique that relies on local fluctuations in the field emission current of a small region of the adsorbate-covered surface. Fluctuations in the field emission current are assumed to reflect diffusion-limited concentration fluctuations in the region of the surface under observation. Gomer has been able to relate the time correlation function of these fluctuations with the local surface diffusion coefficient through a characteristic decay time that can be measured experimentally.[71] This method has been used to provide direct evidence for tunneling in the surface diffusion of hydrogen and deuterium on the (110) plane of tungsten.[72,73]

7.2.2. Sputtering, Nucleation, and Electron Sources

The field emission technique can observe and characterize surface processes on a nanometer scale as a function of local crystallography. This unique capability has been used to investigate a number of difficult problems. For example, field emission microscopy has been used to determine the absolute abundance of chemisorbed species removed by the electron-

[69] C. Kohrt and R. Gomer, *Surf. Sci.* **24**, 77 (1971); **40**, 71 (1973).
[70] C. Wang and R. Gomer, *Surf. Sci.* **74**, 389 (1978).
[71] R. Gomer, *Surf. Sci.* **38**, 373 (1973).
[72] R. DiFoggio and R. Gomer, *Phys. Rev. Lett.* **44**, 1258 (1980).
[73] R. DiFoggio and R. Gomer, *Phys. Rev. B* **25**, 3490 (1982).

stimulated-desorption (ESD) process.[56,74-76] A conventional ESD measurement uses a mass spectrometer to detect ions desorbed from the surface. The measurement technique discriminates against neutral species. An FEEM measurement determines the amount of adsorbate remaining on the surface after ESD by measuring a change in work function. As a result, it does not discriminate against neutral species. Field emission is very sensitive to a change in work function. This means that ESD cross sections as low as 10^{-21} cm^2 can be determined. If a probe-hole FEEM is employed, ESD cross sections for a variety of individual crystal planes can be determined during a single experiment.

Sputtering yields, sputtering rates, and threshold energies for sputtering can also be investigated with field emission techniques.[56,77-79] Threshold energies are determined by measuring the roughness of a field-emitter surface as a function of sputtering energy. The onset of surface roughness appears as a change in the field voltage proportionality factor KR [Eq. (7.1.5)], which can be determined from the slope of the Fowler–Nordheim curve. Sputtering yields and sputtering rates are difficult to assess quantitatively but may be inferred from work function changes associated with the removal of a previously adsorbed metallic layer during the sputtering process.

The process of surface self-diffusion can be examined by measuring the blunting rate of a field-emitter tip as a function of temperature.[80-83] Transmission electron microscopy is used to obtain the emitter profile and the rate of change of the emitter-tip radius. The change in the field emission pattern due to the removal of atomic planes by thermal migration is used to monitor the rate at which an emitter tip changes length.[81]

Nucleation phenomena can be examined by field emission microscopy. The Cu–W, Ag–W, Fe–W, and Zr–W systems have been investigated[84-86] and have yielded new information about this important process.

[74] C. J. Bennette and L. W. Swanson, *J. Appl. Phys.* **39**, 2749 (1968).
[75] D. Menzel and R. Gomer, *J. Chem. Phys.* **41**, 3311. (1974).
[76] W. Ermrich, *Philips Res. Rep.* **20**, 94 (1965).
[77] R. W. Strayer. E. C. Cooper, and L. W. Swanson, *Proc. 25th Annu. Conf. Phys. Electron., Cambridge Mass.*, p. 150 (1965).
[78] C. J. Bennette *NASA Res. Rep.* **NA53-8900** (1967).
[79] H. Vernickel, *Z. Naturforsch., A* **21A**, 1308 (1966).
[80] J. L. Boling and W. W. Dolan, *J. Appl. Phys.* **29**, 556 (1958).
[81] J. P. Barbour, F. M. Charbonnier, W. W. Dolan, W. P. Dyke, E. E. Martin, and J. K. Trolan, *Phys. Rev.* **117**, 1452 (1960).
[82] A. J. Melmed, *J. Appl. Phys.* **38**, 1885 (1967).
[83] P. C. Bettler and F. M. Charbonnier, *Phys. Rev.* **119**, 85 (1960).
[84] A. J. Melmed, *J. Appl. Phys.* **36**, 3585 (1965).
[85] E. Sugata and K. Takeda, *Phys. Status Solidi* **38**, 549 (1970).
[86] A. J. Melmed, *Surf. Sci.* 7, 478 (1967).

Since a field-electron emitter is a high-brightness, point source of near-monochromatic electrons, it is an ideal source for electron optical instruments. The success of field emission sources in this regard is well documented by the commercial availability of high-resolution scanning electron microscopes using field-emitter tips.[87,88] It is interesting to note that the clean, high-vacuum conditions necessary for long emitter lifetimes and maximum current stability have led to a significant improvement in the vacuum environment within commercial instruments.

Further application of field-emitter technology to submicron photolithography, Auger and x-ray microprobe analyzers, laser-irradiated microwave diodes, microwave amplifiers, and flash x-ray devices seems quite promising.[89,90] Macroscopic field emission cathodes consisting of an ordered array of many thousand field emission tips have been used as a source of relativistic electrons in prototype inertial confinement fusion reactors[91] and for pulsed e-beam annealing of semiconductor surfaces.[92]

7.2.3. Electrical Breakdown in High Vacuum

Two metal electrodes placed a fixed distance apart in high vacuum will withstand a certain potential difference V_B applied between them. The quantity V_B is called the "breakdown voltage" of the vacuum gap, and depends upon the geometry of the electrodes and their surface characteristics. If V_B is exceeded, the gap will "break down," a phenomenon characterized by a rapid decrease in the gap impedance as a plasma rapidly expands from the cathode to the anode. Although the breakdown process is not entirely understood, it appears to be initiated by field-electron emission from microscopic protrusions on the cathode surface.[93] Such asperities are probably formed during fabrication, and may actually exist as extrusions of electrode material in the plane of the surface.[94] As V_B is approached, the electrostatic field stress at the cathode surface can erect the extrusions, so that field emission from their apexes may be initiated.[94] Statistically, the asperities should have a range of apex radii, so that each will begin to emit at a different

[87] A. V. Crewe, J. Wall, and L. M. Welter, *J. Appl. Phys.* **39**, 5861 (1968).
[88] A. V. Crewe, M. Isaacson, and D. Johnson, *Rev. Sci. Instrum.* **40**, 241 (1969).
[89] L. O. Hocker, D. R. Sokoloff, V. Danev, A. Szoke, and A. Javan, *Appl. Phys. Lett.* **12**, 401 (1968).
[90] W. P. Dyke, *IRE Trans. Mil. Electron.* **MIL-4**, 38 (1960).
[91] G. Yonas, *Sci. Am.* **239**, 50 (1978).
[92] A. C. Greenwald, A. R. Kirkpatrick, R. G. Little, and J. A. Minnucci, *J. Appl. Phys.* **50**, 783 (1979).
[93] D. W. Williams and W. T. Williams, *J. Phys. D* **5**, 280 (1972).
[94] R. P. Little and S. T. Smith, *J. Appl. Phys.* **36**, 1502 (1965).

applied potential. The prebreakdown current[95] measured between the electrodes as V_B is approached reflects the integrated current from a collection of asperities with the smallest radii. It should be noted that several asperities of different radii, emitting electrons simultaneously, will produce a current–voltage characteristic that will obey the Fowler–Nordheim equation.

Field-emitted electrons having acquired an energy of 80–100 eV can efficiently ionize residual gas atoms in the electrode gap. The field emission current that strikes the anode can also desorb weakly bound surface species that can subsequently be ionized, producing a current of positive ions in the gap. If a dc voltage is applied to the gap, these ions will have time to accelerate to the cathode where they can enhance the field emission process by reducing space charge or by sputter desorbing cathode material. If a short-duration voltage pulse is applied to the gap, then the ions formed in the gap may not have sufficient time to reach the cathode before the voltage terminates. The result may be an apparent increase in the breakdown voltage of the gap. If the voltage pulse vaporizes cathode asperities by intense joule heating, a rapid increase in field emission current during the pulse can be observed.[96]

A breakdown event may be beneficial by "conditioning" the electrodes to withstand subsequently higher voltages. Presumably, the effect is caused by destroying cathode asperities of small radii, or by cleaning the anode surface by electron bombardment. Unfortunately, a breakdown event may also be harmful by sputter-damaging the cathode, thereby producing sharper asperities and a lower breakdown voltage. The breakdown mechanism in vacuum is obviously quite complicated and is critically dependent on the surface condition of the electrodes.

Since field emission appears to play a dominant role in the breakdown mechanism, it is not surprising that field emission microscopy has been used to characterize prebreakdown phenomena.[20] The rationale for such studies is based on the premise that cathode protrusions are responsible for initiating breakdown, and a field-emitter tip is an excellent approximation to an isolated cathode protrusion. It should be noted that electrical breakdown in a field emission microscope is simulated by biasing the tip to a positive potential. The electrostatic stress generated at the tip surface by the applied field can cause the emitter to fracture along crystallographic imperfections. The energy stored in the capacitance of the tip leads then vaporizes the tip surface leading to damage that can be observed in the FEEM.

It is interesting to speculate if and how breakdown would occur if all cathode asperities could be eliminated. A clue may appear in a study of anode phenomena prior to breakdown.[97] Under prebreakdown conditions,

[95] T. Kelsey, *J. Phys. D* **5**, 569 (1972).
[96] N. V. Belkin and E. A. Avilov, *Sov. Phys.—Tech. Phys. (Engl. Transl.)* **15**, 1339 (1971).
[97] J. A. Panitz, *J. Appl. Phys.* **44**, 372 (1973).

anode species are often observed in the gap. These species are presumably created at very sharp anode protrusions by the process of field ionization or field desorption, which will be discussed shortly. In the absence of cathode asperities the breakdown process will be anode dominated and will occur at field strengths of about an order of magnitude higher than conventionally observed.

7.2.4. Molecular Imaging

The simplicity of the field-electron-emission microscope, its intrinsically high magnification, and its nanometer resolution are ideal qualifications for imaging individual molecules. Successful imaging of a single molecule presupposes that the molecules change the local work function of the surface in such a way as to reflect the true contour of the adsorbed species in an FEEM image. Since any adsorbed species can affect the local work function, it is important to eliminate contaminant species during imaging. This precludes the possibility of depositing the molecule of interest by any procedure that requires removing the tip from its ultrahigh-vacuum environment. Nevertheless, such procedures have been suggested[98] and even attempted.[99,100]

The first experiments with molecular imaging in the FEEM were reported by Müller[101,102] in 1950. He used the organic dye copper-phthalocyanine ($C_{32}H_{16}N_8Cu$) because it could be sublimed onto a clean field-emitter tip in high vacuum. Striking high-contrast images were obtained (Fig. 8a) in which fourfold symmetry, characteristic of the planar phthalocyanine molecule (Fig. 8b), could be seen. Müller's conclusion that the fourfold symmetric images represented the shape of the phthalocyanine molecule received widespread attention.[103,104] Surprisingly, the images were 10–20 times larger than predicted from the most optimistic magnification calculations (Eq. 7.1.7). Furthermore, the apparent resolution was almost an order of magnitude better than expected. Müller[102] explained both effects in terms of a locally enhanced magnification, caused by a divergence of electron trajectories in the vicinity of the adsorbed molecule.[105] Later, Rose[31] showed that a perfectly conducting hemispherical protrusion of radius r_0 on a tip of apex

[98] H. Montague-Pollack, *Abstr. 11th Int. Field-Emiss. Symp., Cambridge, Engl.*, p. 23 (1964).

[99] R. C. Abbott and W. Livingston, Jr., *Abstr. University Park, Pa.*, p. 59 (1965). Unpublished.

[100] R. C. Abbott, *Rev. Sci. Instr.* **36**, 1233 (1965).

[101] E. W. Müller, *Naturwissenschaften* **14**, 333 (1950).

[102] E. W. Müller, *Z. Naturforsch., A* **5A**, 473 (1950).

[103] E. W. Müller, *Life* **28**, (June 19), 67 (1950).

[104] E. W. Müller, *Sci. Am.* **186**, 58 (May 1952).

[105] Since most organic molecules are insulators or, at best, semiconductors, this explanation is only qualitatively correct.

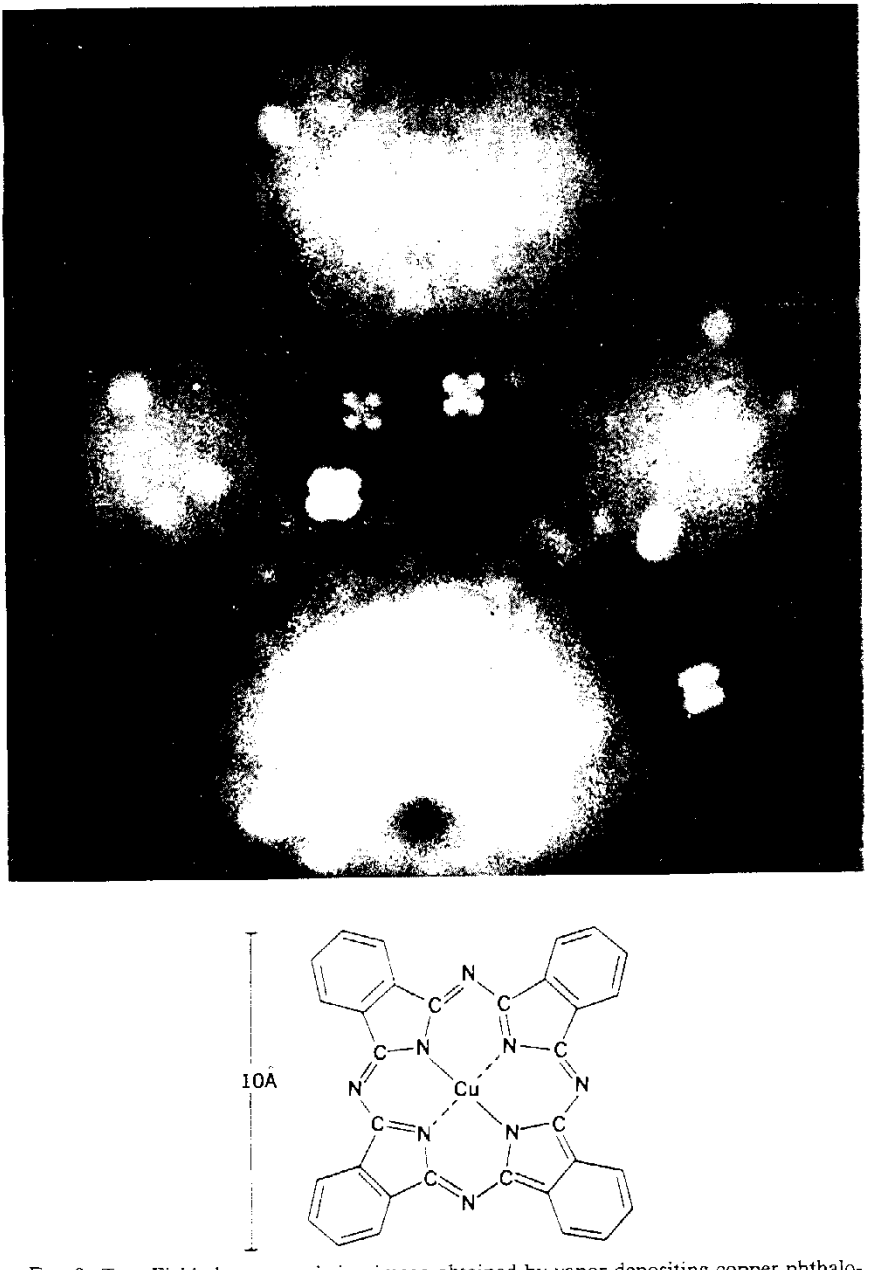

FIG. 8. Top: Field-electron-emission image obtained by vapor depositing copper phthalocyanine ($C_{32}H_{16}N_{18}Cu$) on a thermally annealed, tungsten field-emitter tip at 77 K. [Courtesy of A. J. Melmed, National Bureau of Standards, Washington, D.C.] Bottom: The structure of the copper phthalocyanine molecule ($C_{32}H_{16}N_{18}Cu$). (From Melmed.[108])

radius R would cause an increase in the normal magnification of the field emission microscope by an amount M_p, where

$$M_p \approx 1.1(R/r_0)^{1/2} M. \tag{7.2.3}$$

For a semiconducting phthalocyanine molecule $r_0 \approx 0.5$ nm, on a tip 160 nm in radius, $M_p = 20M$, in apparent agreement with the FEEM image size. Figure 8a shows that a range of discrete image sizes and intensities is actually seen. Other observations indicated that these effects were due to the number of phthalocyanine molecules adsorbed at a single location on the surface.[106,107] The larger, more intense "quadruplet" images were interpreted as a planar stacking of many individual molecules of common orientation to form a phthalocyanine "crystallite." The smaller, less intense, images were thought to reflect only a few stacked molecules. Twofold symmetric images, or "doublets," were associated with a single molecule standing on edge.[106-108]

Gomer and Speer[109] measured the current–voltage characteristic of individual quadruplets caused by the adsorption of zinc-phthalocyanine. When compared with theory, their measurements gave a reasonable ionization potential for the molecule (7 ± 0.5 eV). This further supported Müller's contention that individual molecules were being imaged. Additional support came from imaging a twofold symmetric molecule, flavanthrene ($C_{28}H_{12}N_2O_2$), which could be vapor deposited on the tip surface. More than 99% of the image features were doublets,[106,108] (Fig. 9a), which apparently reflected the known symmetry of the molecule (Fig. 9b).

Unfortunately, when a large number of organic molecules of other shapes were examined, only quadruplet and doublet images were seen.[108,110-113] It appeared that field-electron-emission images were not displaying the actual contour of an individual adsorbate but rather some characteristic common to all of them. Müller[108] suggested that the images might result from a complicated diffraction phenomenon caused by an interaction between the adsorbed molecule, the substrate, and the tunneling electrons. Still later, he associated the appearance of the image with the presence of π-electrons in the molecule. He suggested that the magnetic moment of the π-electrons should

[106] A. J. Melmed and E. W. Müller, *J. Chem. Phys.* **29**, 1037 (1958).
[107] A. J. Melmed, USAF Tech. Rep. AFOSR TN 58-646 (1958) (ASTIA AD No. 162 178).
[108] J. Melmed, *in* "Field-Ion Microscopy" (J. J. Hren and S. Ranganathan, eds.) p. 211 (Plenum Press, New York, 1968).
[109] R. Gomer and D. A. Speer, *J. Chem Phys.* **21**, 73 (1953).
[110] P. Wolf, *Z. Angew. Phys.* **6**, 529 (1954).
[111] E. Hörl and F. Strangler, *Acta Phys. Austriaca* **10**, 1 (1956).
[112] J. A. Becker and R. G. Brandes, *J. Appl. Phys.* **27**, 221 (1956).
[113] R. Haefer, *Acta Phys. Austriaca* **8**, 105 (1953).

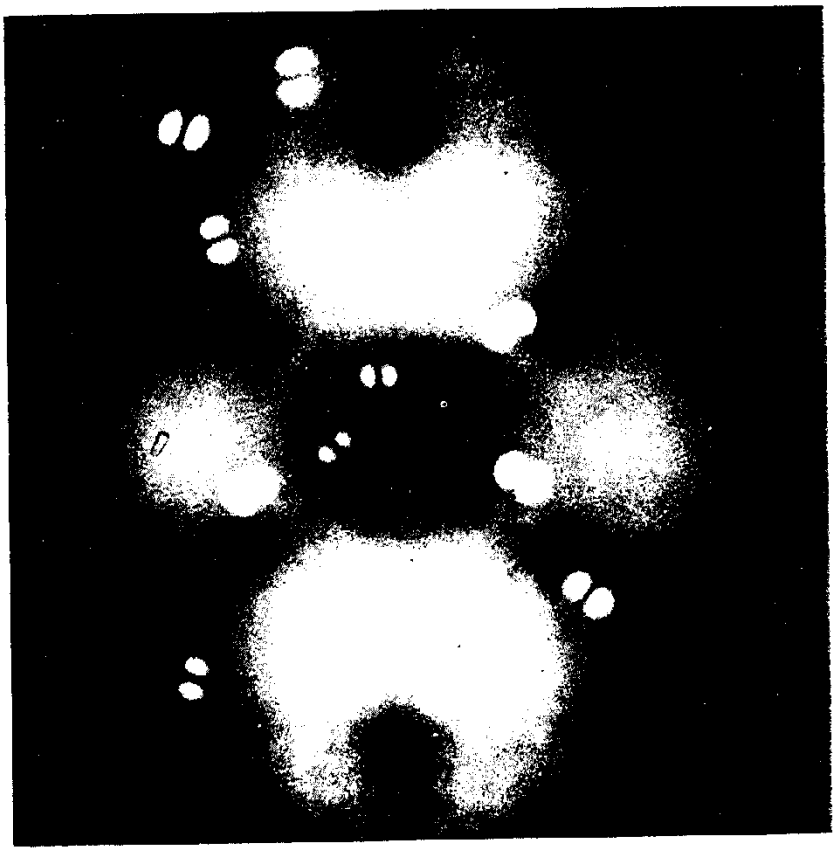

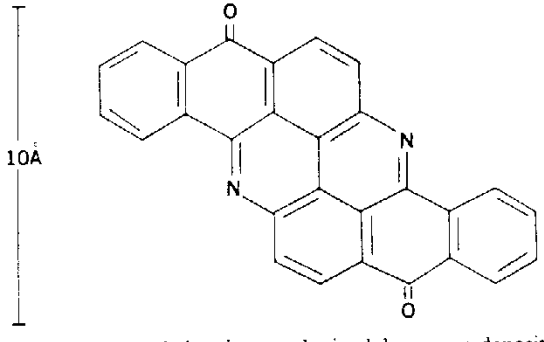

FIG. 9. Top: Field-electron-emission image obtained by vapor depositing flavanthrene ($C_{28}H_{12}N_2O_2$) on a thermally annealed tungsten field-emitter tip at 77 K. [Figure courtesy of A. J. Melmed (The National Bureau of Standards, Washington, D.C.).] Bottom: The structure of the flavanthrene molecule. (From Melmed.[108])

interact strongly with the spin of the slow-moving, field-emitted electrons.[114] The resulting interaction could cause a splitting of the field-emitted-electron beam. However, Müller's model could not explain the formation of a four-fold symmetric beam required for the production of quadruplet images.

Hörl and Strangler[111] proposed that the images had nothing to do with an adsorbed molecule but were caused by clusters of tungsten atoms displaced from the substrate during molecular deposition in the presence of a high field. Since identical image features were also obtained after deposition in the absence of a field, Hörl and Strangler's explanation was largely ignored. It is conceivable that the images could result from a decomposition product common to all of the imaged species, but this is unlikely in view of the large number of different molecular structures and substrates that were examined.

Melmed[115] proposed that an adsorbed molecule or a molecular crystallite could act as an "aperture" in which the probability of electron emission would be larger than that of the surrounding clean surface. He qualitatively argued that field-emitted electrons might interact with an excess negative charge distribution associated with the polarized molecule, splitting the electron trajectories into two or four equally intense bundles. The exact mechanism responsible for splitting the beam was not explained.

An alternate possibility, consistent with the hypothesis that the adsorbed molecules stack to form an ordered crystallite, was advanced by Giaever.[116] He suggested that doublet images are caused by electrons emitted from single planar molecules standing on edge, whereas quadruplet, and more infrequently, esoteric patterns are caused by emission from the ends of small molecular crystallites (Fig. 10). Giaever believed that under certain conditions a field emission pattern could reflect the presence of an individual molecule but not its actual morphology. He interpreted a common symmetry in the emission pattern of different molecules in terms of a common symmetry in the electric field distribution surrounding any planar adsorbed species.

7.2.5. Single-Atom Imaging

The possibility that the FEEM may have sufficient resolution to image single atoms was raised during the time that molecular imaging was in vogue. Müller[102] proposed that "granulation" observed in an FEEM image of a tungsten following barium deposition was due to enhanced emission at individual barium atoms. Becker[117,118] questioned this interpretation, pre-

[114] E. W. Müller, Electron Microsc. Soc. Am., 1953 (unpublished lecture). See ref. 21, p. 139.
[115] A. J. Melmed, Ph.D. Thesis, Pennsylvania State Univ., University Park, 1958.
[116] I. Giaever, *Surf. Sci.* **29**, 1 (1972).
[117] J. A. Becker, *Bell Syst. Techn. J.* **30**, 907 (1951).
[118] J. A. Becker, *Prgm. 1st Int. Field-Emiss. Symp., McMinnville, Or.* (1952). Unpublished.

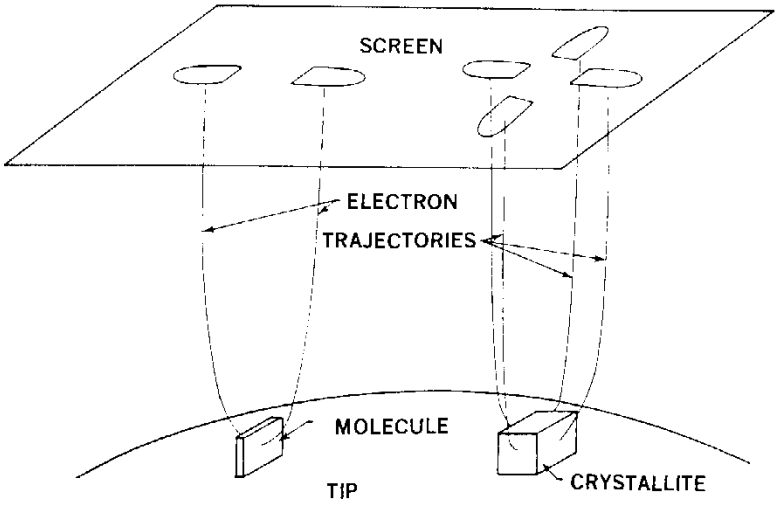

FIG. 10. "A schematic drawing of electron emission from molecular objects adsorbed on a field-emitter tip. For clarity, the sizes of the molecular objects and the tip itself have been drawn grossly magnified. The separation of the electron trajectories is due to the local field distortion around the molecules." (Figure and caption from Giaever.[116] Copyright North-Holland Physics Publishing, Amsterdam.)

ferring to regard the granulation as enhanced emission from clusters of several barium atoms. Ashworth[119] found that if hydrogen was introduced into a well-baked FEEM, single image spots could be observed on flat smooth crystal faces that had a low work function. Eventually, each spot would appear to split into two halves. These remained close together, and would usually rotate about each other before disappearing. Alternatively, the individual image spots would not disappear but would move randomly away from each other over the surface. If argon was adsorbed, only single image spots were observed. Ashworth believed that the FEEM images of molecular hydrogen reflected dissociation of the adsorbate. After dissociation, two image spots were observed, suggesting that two hydrogen atoms (visible as separate entities) moved randomly across the surface. Since argon does not adsorb as a molecular species, only single image spots would be seen. A smooth flat surface of low work function was required to see an image, because on such a surface an adsorbate would produce the maximum perturbation in the surface potential. This would lead to enhanced emission and image contrast and an increase in local magnification and resolution.[30-32]

The goal of imaging individual atoms in the FEEM was never completely

[119] F. Ashworth, Ph.D. Thesis, Univ. of Bristol, Bristol, England, 1948.

achieved. Nevertheless, it was this challenge that ultimately led Müller to develop the field-ion microscope in which single atoms can unambiguously be observed.

7.3. Field-Ion Microscopy

In theory, any ionization mechanism that can be localized to the immediate vicinity of a surface species can be used to image that species. By applying a dc bias to the tip surface, the resulting ions can be forced to follow almost radially directed field lines, which leads to a magnified image of their point of origin. As early as 1941, Müller observed [120] that adsorbed barium atoms could be removed from a tungsten field emission tip by reversing the polarity of the tip bias and increasing the field strength beyond 8 V nm^{-1}. He later reasoned [121] that if the desorption process involved the formation of positive barium ions, these ions might yield a magnified image of their adsorption sites on the surface. (If neutrals were formed by the desorption process they would not be accelerated in the applied field and no magnification would

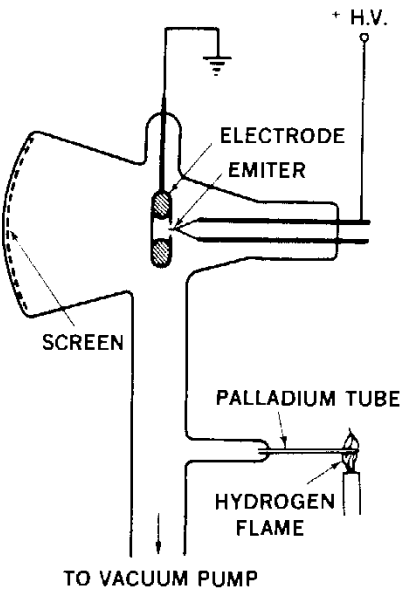

FIG. 11. A schematic drawing of the original room-temperature field-ion microscope introduced by E. W. Müller in 1951. (From E. W. Müller and T. T. Tsong,[126] "Field-Ion Microscopy: Principles and Applications." Copyright 1969 by American Elsevier Publishing Co.)

[120] E. W. Müller, *Naturwissenschaften* **29**, 533 (1941).
[121] E. W. Müller, *Z. Phys.* **131**, 136 (1951).

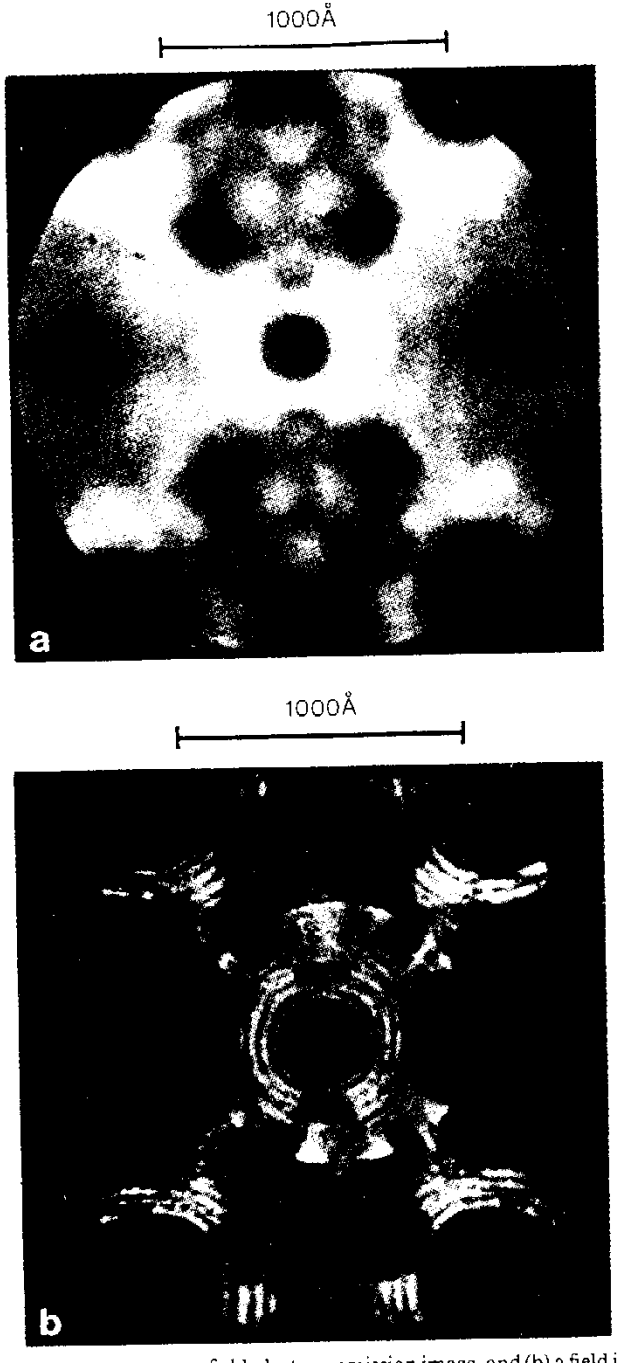

FIG. 12. (a) A room-temperature field-electron-emission image, and (b) a field ion image of a tungsten tip ($R = 940$ Å) taken by E. W. Müller in 1951. The almost concentric, diffuse circle of light at approximately one-half of the image diameter was attributed to secondary electrons released by hydrogen-ion bombardment of an annular cathode placed opposite the tip. (From Müller.[121])

result.) The desorption process produces very small ion currents. Even a monolayer of surface species desorbed as positive ions from the entire surface of the tip would yield only 10^{-14} C of charge.

Müller[121] observed that for a barely discernable image on a fluorescent screen an image intensification of at least 10^6 would be required. Since modern methods of image intensification were not available, this could be achieved only by a rapid succession of adsorption–desorption sequences, with the resulting images photographically integrated. It would be convenient to supply the imaging species from the gas phase so that a continuous supply would be available for adsorption onto the tip surface. Hydrogen was selected for this purpose and introduced into an existing FEEM by diffusion through a heated palladium tube (Fig. 11). Müller believed that if the emitter tip was kept at a sufficiently high positive bias in the presence of ambient hydrogen, an adsorption–desorption cycle could be indefinitely maintained. We now know that field ionization of gas-phase hydrogen in free space was actually responsible for the images that Müller observed (Fig. 12). But, fortuitously, the right conditions were established, and a truly revolutionary microscopy was born.[121]

7.3.1. Field Ionization

Field ionization of an isolated atom in free space by electron tunneling was first proposed by Oppenheimer[122] in 1928. By formulating the problem quantum mechanically, he was able to demonstrate that the lifetime of an electron in an isolated hydrogen atom depended upon the magnitude of an external electric field. At fields of the order of 1 V cm^{-1}, the calculated lifetime was greater than any estimate of the age of the universe, but at fields approaching 15 V nm^{-1}, ionization would occur within a time frame of less than one second. Although Erying *et al.*[7] applied positive fields to their emitter tips in 1928, they did not observe a positive ion current because their experiments were performed in high vacuum.

In 1931, Lanczos[123] explained field-induced quenching of spectral lines in the Stark effect by quantum mechanical tunneling from an excited state of the hydrogen atom. Guerney[124] considered the tunneling process to be an explanation of the neutralization of hydrogen ions at the cathode of an

[122] J. R. Oppenheimer, *Phys. Rev.* **31**, 67 (1928).
[123] C. Z. Lanczos, *Z. Phys.* **68**, 204 (1931).
[124] R. W. Gurney, *Proc. R. Soc. London, Ser. A* **134**, 137 (1932).

electrolytic cell. He noted that tunneling should occur at a critical distance from the electrode surface where the ground state energy of the atom was equal to the Fermi level of the metal. However, the field-ion imaging process could not be explained until Inghram and Gomer[125] developed a theoretical description of field ionization in the vicinity of a metal surface. They clearly showed that hydrogen was not ionized on the emitter surface but in free space. Field-ion images were produced by a gas-phase ionization process and not by an adsorption–desorption cycle at the surface of the tip.

In free space, the valence electron of a neutral atom can be considered as bound in a potential well. An energy I (equal to the ionization potential) must be supplied in order to ionize the atom. In an electric field, the potential well will be distorted, with the side of the well toward the anode reduced in width. As the electric field strength is increased, this width will become comparable to the de Broglie wavelength of the valence electron in the atom, and the probability for tunneling through the potential barrier will greatly increase. As the distance between the atom and the anode is decreased, the barrier width will decrease, due to short-range contributions to the potential from atom–surface interactions.

Since tunneling can occur only into an unoccupied state of the metal, the ground state of the valence electron in the atom must lie above the Fermi level of the metal. This condition (shown schematically in Fig. 13) is satisfied at some critical distance X_c from the metal surface, where

$$eFX_c = I - \Phi. \tag{7.3.1}$$

The image potential due to the tunneling electron (and the change in the polarization energy of the atom upon ionization) have been omitted in Eq. (7.3.1) because their combined contribution is usually negligible. For hydrogen $I = 13.5$ eV. In a field of 2 V nm^{-1} above a tungsten surface (for which $\Phi = 4.5$ eV), the critical distance for ionization $X_c = 0.45$ nm.

A reasonably accurate estimate of the ionization probability of an atom at the critical distance can be obtained by multiplying the probability of an electron tunneling from the atom by the frequency with which it strikes the tunneling barrier. The former can be estimated from the WKB approximation using a simplified triangular barrier. The latter can be estimated from the Bohr model using an "effective" nuclear charge appropriate to the atom in question.[126] The field-ion current that is measured should then be the

[125] M. G. Inghram and R. J. Gomer, *J. Chem. Phys.* **22,** 1279 (1954).

[126] E. W. Müller and T. T. Tsong, "Field-Ion Microscopy: Principles and Applications." Am. Elsevier, New York, 1969.

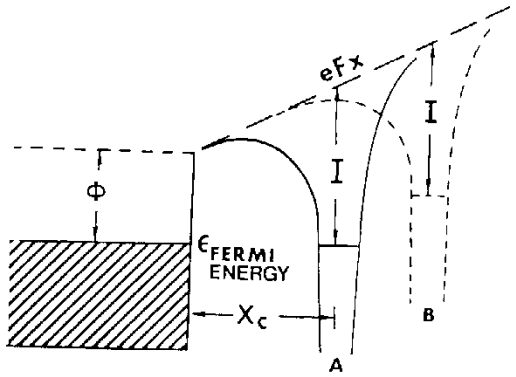

FIG. 13. A schematic drawing of the field-ionization process. At position A, the atom is located at a distance X_c from the metal surface. X_c is the critical distance for field ionization, and corresponds to the position at which the energy level of the valence electron in the atom is equal to the Fermi energy of the metal. At closer distances to the surface, the energy level of the electron will lie below the Fermi energy so that tunneling will not occur. For distances far from the surface (e.g., position B) the barrier width will be large, so that tunneling will be improbable. (From Panitz.[27a] Copyright 1982 The Institute of Physics.)

product of the ionization probability of an atom (assumed to be isotropic) and the number of atoms that arrive in the ionization zone each second. It was noticed quite early that the measured field-ion current was at least an order of magnitude larger than expected if a supply of imaging gas molecules governed by the kinetic theory of gases and an ionization probability of 100% was assumed. The paradox was resolved when it was realized that the number of gas-phase molecules in the vicinity of the tip is artificially enhanced by field-induced dipole attraction to the tip apex. When calculated values for the enhancement factor due to the field-induced dipole energy αF^2 (α = the polarizability) were performed,[127-129] field-ion currents in good agreement with the measured values were obtained.

7.3.2. Field-Ion Energy Distributions

The energy distribution of field-ionized gas atoms can provide valuable insight into the nature of the ionization process. If an ion is created at the emitter-tip surface, it will acquire a kinetic energy corresponding to its acceleration through the full potential difference that is applied between the tip and a suitable collector. If the ion is created in space at some distance from

[127] M. J. Southon, Ph.D. Thesis, University of Cambridge (1963).
[128] E. W. Müller and K. Bahadur, *Phys. Rev.* **102**, 624 (1956).
[129] E. W. Müller, *Adv. Electron. Electron Phys.* **13**, 83 (1960).

the surface, it will acquire less kinetic energy in traveling to the collector. Therefore, the threshold energy in a field-ion energy distribution will indicate the position at which the ions are formed, and the width of the energy distribution will reflect the spatial extent of the ionization region.

The first field-ion energy distribution was measured in 1954 by Inghram and Gomer[125] using a mass spectrometer that incorporated a field-ionization source. From the width of their mass peaks, they concluded that the width of the energy distribution for field-ionized hydrogen was less than 20 eV, the resolution of their instrument. At very high fields they noticed that the distribution broadened, indicating spatial ionization far from the tip surface. By using an improved analyzer with an energy resolution of ~2 eV, Müller and Bahadur[128,130] found that the half-width of the energy distribution for field-ionized argon was ~2 eV, with a sharp threshold indicating spatial ionization ~0.5 nm above their tungsten surface. These measurements were extended by Tsong and Müller[131] who investigated a number of gases including helium. Figure 14 shows several typical energy distributions for field-ionized helium as a function of the potential applied to the tip. The width of the distribution at 20 kV (corresponding to $F = 45$ V nm^{-1} and the best visual image) indicates that the region of ionization is less than 0.02 nm

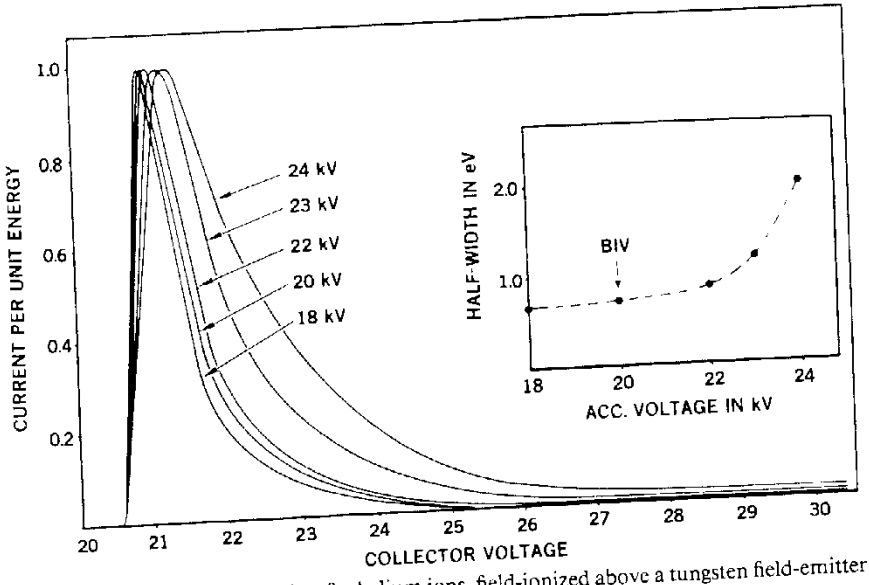

FIG. 14. An energy distribution for helium ions, field-ionized above a tungsten field-emitter tip. (From Tsong and Müller.[131])

[130] E. W. Müller and K. Bahadur, *Phys. Rev.* **99**, 1651 (1955).
[131] T. T. Tsong and E. W. Müller, *J. Chem. Phys.* **41**, 3279 (1964).

thick or only a few tenths of the diameter of the ionizing gas atom. Similar results were found for neon, argon, and hydrogen. As the field strength was increased, the distributions broadened toward lower energies, in agreement with Inghram and Gomer's earlier observations. Jason *et al.*[132] subsequently discovered a weak periodic structure in the low-energy tail of hydrogen and neon distributions. Jason[133] and Aiferieff and Duke[134] interpreted the multiply peaked structure as a resonance associated with the tunneling of an electron between the ionizing atom and the nearby metal surface. The resonance model predicted an increase in peak spacing with applied field, as well as a progressive decrease in peak spacing toward lower energies. Both effects were observed experimentally but at a significantly higher field strength than predicted. Lucas (unsuccessfully) attempted to explain the experimental observations in terms of an excitation of multiple surface plasmons.[135,136]

In order to examine what had become known as the "Jason effect" in more detail, Müller and Krishnaswamy[137] measured the field-ion energy distributions caused by a single atom on smooth and rough crystal planes. Jason had averaged the ion current over a large region of the tip surface so that the effect of surface morphology could not be determined. By using a probe hole to limit the field of view to a single atomic site and a high-resolution energy analyzer, Müller and Krishnaswamy found as many as seven Jason peaks above the close-packed planes of tungsten and iridium but only two or three above the more open "structured" planes [such as the (111)]. For highly disordered surfaces of carbon and silicon, it was difficult to detect more than one peak in the energy distribution.

These measurements indicated that the atomic roughness of a surface could reduce or even eliminate the Jason effect. Intuitively, the phenomenon is easy to understand. Imagine that the electron that tunnels from an atom ionizing in space has a finite probability of being reflected from the nearby metal surface and essentially zero probability of tunneling back into the resulting ion. Under such conditions, standing waves will exist in the potential well defined by the ionizing atom and the surface. The strength of the resulting resonances (which are reflected by the Jason peaks) will depend on the uniformity of the surface potential that governs the electron reflectivity at the metal surface. The smoother the surface, the more uniform the potential, and the greater will be the probability for electron reflection necessary to produce the Jason effect.

[132] A. J. Jason, R. P. Burns, and M. G. Inghram, *J. Chem. Phys.* **43,** 3762 (1965).
[133] A. J. Jason, *Phys. Rev.* **156,** 156 (1967).
[134] M. E. Aiferieff and C. B. Duke, *J. Chem. Phys.* **46,** 938 (1967).
[135] A. A. Lucas, *Phys. Rev. Lett.* **26,** 813(1971); *Phys. Rev. B* **4,** 2939 (1971).
[136] A. A. Lucas and M. Sunjic, *J. Vac. Sci. Technol.* **9,** 725 (1972).
[137] E. W. Müller and S. V. Krishnaswamy, *Surf. Sci.* **36,** 29 (1973).

At very high field strengths (above 50 V nm^{-1}) Müller and Krishnaswamy[137] found that a few percent of the field-ionized noble gas atoms had energies higher than the threshold energy of the distribution. It appeared as though some imaging gas molecules were being ionized within the critical distance from the surface—within the so-called "forbidden zone." In order to ionize an atom within the forbidden zone, energy must be supplied to raise the level of the valence electron in the atom above the Fermi level of the metal. Müller and Krishnaswamy believed that this energy was supplied by a continuous current of low-energy electrons striking the tip surface. The electron current is presumably produced by spatial ionization of imaging gas atoms far from the tip.[137] Imaging gas atoms are found on the tip because they are bonded to its surface by a short-range field-induced dipole–dipole bond.[138] This unique type of bonding occurs only at fields greater than 10 V nm^{-1}. The process is called "field adsorption." It was discovered experimentally by Müller *et al.*[139] in 1969 and explained theoretically by Tsong.[140]

7.3.3. The Hopping Gas Model

Field-ion energy distribution measurements localized the region of greatest ionization probability to a volume of space located above the field-emitter surface. At a certain electric field strength (called the best-image field), the ionization region separates into "disks" of high ionization probability associated with each of the more protruding atoms of the surface. At these positions the local electric field strength is greatest. Field-ion energy distributions indicate that the ionization disks are of the order of 0.02 nm thick and are approximately equal in diameter to an imaging gas atom. At the best-image field, the field-ion image will display maximum surface detail and definition over the widest field of view. The best-image field is established by applying a potential difference between the emitter tip and the screen, which is known as the "best-image voltage" or BIV. Although BIV is subjectively chosen, different observers always select the same BIV to within a few percent.

Since the imaging gas molecules are polarized in the inhomogeneous field above the emitter surface, they will eventually strike the emitter with a dipole attraction velocity $(\alpha/m)^{1/2}F$, which is much larger than kT. If they do not condense on the tip surface, the imaging gas molecules will lose some fraction of this energy (determined by their thermal accommodation coefficient) and rebound, only to be attracted once again by polarization forces. At BIV, a reasonable fraction of the emitter-tip surface will be covered with field-ad-

[138] E. W. Müller, *J. Less-Common. Met.* **28**, 37 (1972).
[139] E. W. Müller, S. B. McLane, and J. A. Panitz, *Surf. Sci.* **17**, 430 (1969).
[140] T. T. Tsong, *Phys. Rev. Lett.* **25**, 911 (1970).

sorbed imaging gas molecules, which greatly enhances the thermal accommodation process.

One can picture the polarized gas-phase molecules as eventually being trapped in a region of space close to the emitter apex while slowly diffusing over the surface of the tip in a random "hopping" motion.[126] At some point, each molecule will pass through the ionization disk above a protruding atom of the surface. If its velocity is sufficiently reduced by the thermal accommodation process, it will dwell in the ionization region and have a finite probability of losing an electron to the metal by the tunneling process. The tunneling probability is enhanced by the presence of field-adsorbed gas atoms at protruding sites directly below the ionization region. If tunneling occurs, the resulting ion will accelerate rapidly away from the tip surface in an almost radial direction. At an imaging gas pressure of several millitorr, some 10^5 ions s^{-1} will be created above each protruding surface atom. This is equivalent to an ion current of the order of 10^{-14} A. The intensity of the resulting field-ion image is roughly equivalent to that of the Milky Way viewed with dark-adapted eyes on a moonless night.

7.3.4. The Low-Temperature Field-Ion Microscope

In thermally accommodating to the tip temperature, an imaging gas species will lose its field-induced dipole energy $\frac{1}{2}\alpha F^2$, so that after ionization its kinetic energy parallel to the tip surface will be

$$\tfrac{1}{2}mv_T^2 \approx kT. \tag{7.3.2}$$

The resolution of the FIM is obtained by combining Eqs. (7.1.5), (7.1.10), and (7.3.2) and noting that the resolution will be ultimately limited by the spatial extent of the ionization zone δ_0, that is,

$$\delta = \delta_0 + (4kT\beta^2 R/KeF)^{1/2} = \delta_0 + A(RT/F)^{1/2}, \tag{7.3.3}$$

where A is essentially constant and δ_0 is of the order of the diameter of the imaging gas ion. All other things being equal, cooling the tip from room temperature to liquid-nitrogen temperature will improve the image resolution by roughly $(80/300)^{1/2} \approx 50\%$.

As early as 1951, Müller[121] noted that "experiments were in progress with helium desorption from strongly cooled tips." However, in 1952 Gomer[141] reported that immersing an entire FIM in liquid nitrogen did not improve the resolution of the image. Apparently, observing the FIM pattern through the cryogenic liquid prevented an improvement in resolution from being noticed. Perhaps as a result, low-temperature experiments were not actually

[141] R. Gomer, *J. Chem. Phys.* **20**, 1772 (1952).

pursued. Fortunately, in 1956 Müller[142,143] noted the great improvement in resolution that could be obtained by cooling the tip. Atomic resolution had been achieved simply by using helium as an imaging gas and cooling only the tip with liquid nitrogen.

For optimum resolution at any tip radius, Eq. (7.3.3) predicts that the tip temperature should be kept as low as possible, the diameter of the imaging gas ion should be chosen to be as small as possible, and the electric field at BIV should be made as large as possible. With a condensation temperature below 5 K, an effective diameter of 0.19 nm and a best-image field of 45 V nm^{-1}, helium is by far the best choice for an imaging gas. However, the mechanical stress exerted on the emitter by the field at helium BIV ($F^2/8\pi = 10^{11}$ dyn cm^{-1}) will elastically deform most materials. Only those that have a relatively high Young's modulus and are free of major lattice defects will survive. With some sacrifice in resolution, other imaging gases or gas mixtures can be selected in order to reduce the field stress at BIV. For example, hydrogen produces a field-ion image at about one-half of helium BIV, reducing the field stress by 50%. By a careful choice of imaging conditions a number of materials have been successfully imaged.[126]

If the tip voltage is raised beyond BIV, the ionization region in front of the tip is extended further into space and becomes laterally delocalized so that the FIM image becomes progressively blurred. As the electric field strength increases it will reach a value sufficiently high to ionize weakly adsorbed surface species and displaced lattice atoms. These will be desorbed from the surface as positive ions. Eventually, even the lattice will begin to dissolve as lattice species become ionized. At a given tip potential and temperature, the surface will eventually assume a stable topography or "end form" of minimum free energy. This surface will be atomically smooth, and can be as crystallographically perfect as the bulk. The removal of lattice atoms in a high electric field is called "field evaporation," in analogy with thermal evaporation, which occurs at high temperatures. Field evaporation was discovered by Müller[142,144] in 1956. It is the only method that can prepare an emitter surface with the atomic regularity required for high-resolution lattice imaging. Field evaporation is a specific case of "field desorption," a term applied to the removal of *any* species in a high electric field. Since a material of interest may field-evaporate at a field strength that is equivalent to (or below) BIV, field evaporation can also prevent stable FIM images from being obtained.

Figure 15 shows a ball model of the apex of a (011)-oriented, bcc field-

[142] E. W. Müller, *Z. Naturforsch.*, **11A**, 87 (1956).
[143] E. W. Müller, *J. Appl. Phys.* **27**, 474 (1956).
[144] E. W. Müller, *Phys. Rev.* **102**, 618 (1956).

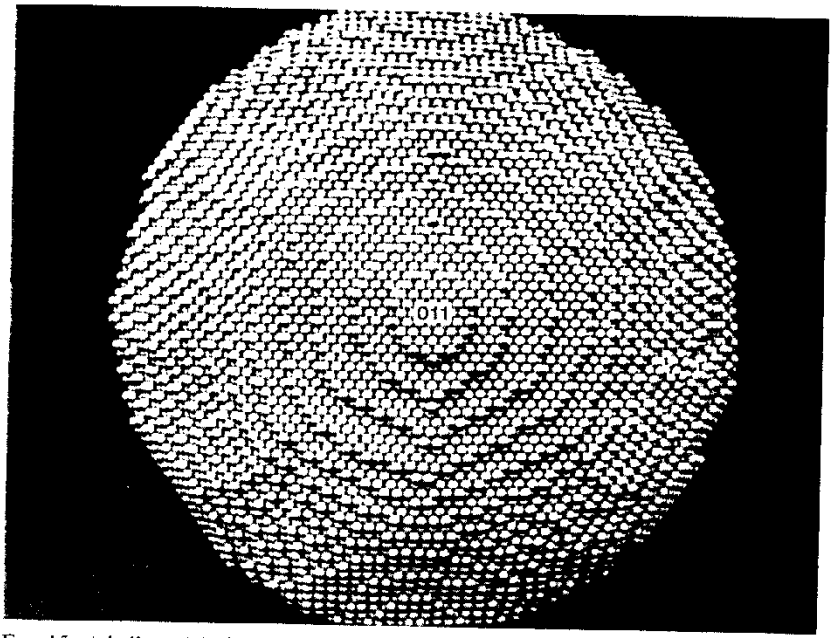

FIG. 15. A ball model of the apex region of a (011)-oriented, bcc field-emitter tip following field evaporation. (From Panitz.[27a] Copyright 1982 The Institute of Physics.)

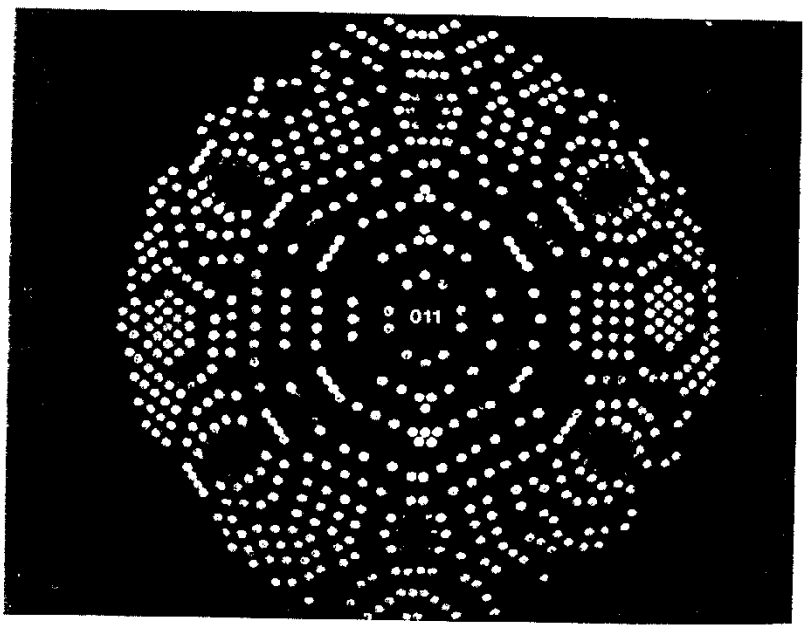

FIG. 16. The ball model of Fig. 15 with the more protruding edge atoms at lattice steps painted with fluorescent dye and photographed in the dark. (From Panitz.[27a] Copyright 1982 The Institute of Physics.)

emitter tip as it would appear after field evaporation if each surface atom could be seen.[129] Since the more protruding atoms exposed at the corners of the lattice steps will generate the highest local fields. these atoms will appear brightest in the field-ion image. In order to simulate a field-ion micrograph, atoms with four next-nearest neighbors can be painted with a bright fluorescent dye, and atoms on slightly less protruding sites can be painted with a weak fluorescent dye.[129] When photographed in the dark, the resulting image (shown in Fig. 16) accurately represents an image of tungsten observed in an FIM (Fig. 17).

Once a stable field-evaporated endform is reached, the tip voltage can be lowered to BIV for imaging, or can be increased gradually to controllably dissect the near-surface region of the lattice, atomic layer by atomic layer. Since the lattice dissolves during field evaporation, bulk artifacts (naturally occurring in the near-surface region or purposely introduced) can be exposed for imaging or removed from the lattice. Field evaporation is the only known method that will produce atomically clean surfaces with complete confidence.

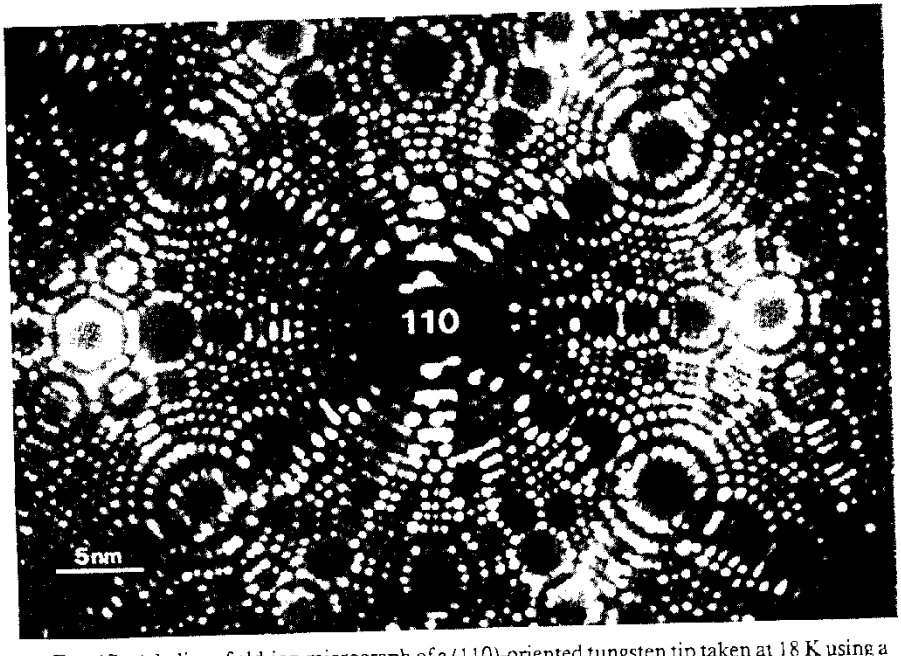

FIG. 17. A helium field-ion micrograph of a (110)-oriented tungsten tip taken at 18 K using a chevron channel-plate image intensifier located within the FIM. (From Panitz.[27a] Copyright 1982 The Institute of Physics.)

7.3.5. The Magnification of a Field-Ion Image

The magnification of a field-ion image will vary slightly across the imaged area because of local variations in the radius of curvature of the tip. Fortunately, a very precise local magnification can be obtained if the FIM image exhibits crystallographic order.[126] If γ is the known apex angle between two imaged, crystallographic directions and n is the number of net plane rings of known step height s that are resolved in the image, then, from Fig. 18, the local radius of curvature is

$$R_L = ns/(1 - \cos\gamma). \tag{7.3.4}$$

For cubic crystals, the step heights of the $\{hkl\}$ poles are given by

$$s = a/\delta(h^2 + k^2 + l^2)^{1/2}, \tag{7.3.5}$$

where a is the lattice constant and $\delta = 1$ or 2 as shown in Table I. For tungsten, an average tip radius (in nanometers) can be obtained by multiplying the number of net plane rings seen in the image between the centers of the (001) and (121) planes by 0.16. Unlike an FEEM image or an electron

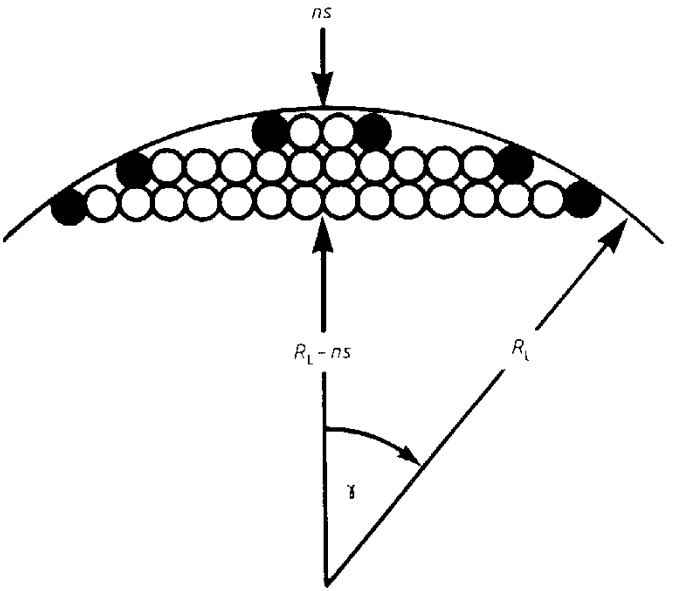

FIG. 18. A schematic drawing of a tip in profile showing two crystallographic directions separated by a known angle γ. R_L is the local radius of curvature of the tip, n is the number of net plane rings seen in the image, and s the known step height per ring (see text). The dark atoms at the edge are those that are seen in an FIM image. (From Panitz.[27a] Copyright 1982 The Institute of Physics.)

TABLE I. The Scaling Factor δ Used to Determine the Step Heights of the hkl Poles in a Field-Ion Image[a,b]

δ	Simple Cubic Lattice	bcc Lattice	fcc Lattice
1	All values of h, k, l	$h+k+l$ even	h, k, l odd
2		$h+k+l$ odd	h, k, l mixed parity

[a] From Panitz.[27a] Copyright 1982 The Institute of Physics.
[b] See Eq. (7.3.5).

micrograph, each resolved field-ion image contains its own magnification standard, which is the crystal lattice itself.

7.3.6. The Modern Field-Ion Microscope

A low-temperature field-ion microscope is a conceptually simple device. A generic form of the instrument is shown schematically in Fig. 19. A cryogenically cooled specimen tip that is biased to a high positive potential is located in an ultrahigh-vacuum environment that can be selectively backfilled to about 10^{-5} Torr with a very pure imaging gas. If helium or neon are used for imaging, a liquid-nitrogen-cooled titanium sublimator provides effective pumping of all background contaminants during the imaging process. Helium or hydrogen can be conveniently introduced into the vacuum chamber by diffusion through a thin-walled electrically heated quartz or palladium thimble. It is not necessary to provide a very pure supply of these species, since larger molecules and other impurities cannot diffuse into the vacuum system.

A fiber-optic faceplate coated with a fluorescent material (such as P1 phosphor) provides a convenient way to record the field-ion image. The faceplate will transmit the image from the vacuum environment to laboratory ambient, where it can be easily photographed.[145] If a contact print is made by pressing a photographic emulsion directly onto the faceplate, optical lenses with their inherent slow speed and distortion can be avoided. Using Polaroid® Type 55 film, a print and a negative can be immediately obtained without the need for darkroom facilities.[146] In many instances images can be quickly recorded without the use of additional image intensification.

One disadvantage of a simple FIM is the relatively long time required to change specimen tips, particularly if ultrahigh-vacuum conditions must be reestablished prior to imaging. In order to overcome this difficulty, the tip can be placed in a prepumped specimen chamber and transferred under vacuum through an isolation valve, to the base of the cryogenic reservoir.[147]

[145] J. J. Hren and R. W. Newman, *Rev. Sci. Instrum.* **38**, 869 (1967).
[146] J. A. Panitz, *Rev. Sci. Instrum.* **44**, 1034 (1973).
[147] J. A. Panitz, *J. Vac. Sci. Technol.* **14**, 502 (1977).

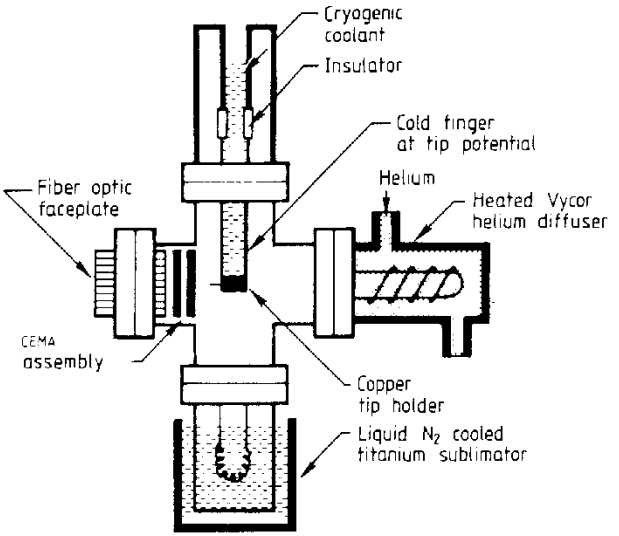

FIG. 19. A schematic drawing of a simple generic form of a modern field-ion microscope. The device is typically constructed from interchangeable stainless steel vacuum components. The chamber is attached to a conventional ultrahigh-vacuum system that is not shown. With this simple microscope, metallic surfaces can be imaged with atomic resolution, and surface processes directly examined as a function of surface crystallography and morphology. (From Panitz.[27a] Copyright 1982 The Institute of Physics.)

Alternatively, a multiple tip holder can be employed so that ten or fifteen tips can be inserted into the vacuum chamber at one time, with each tip individually selectable for imaging.[148]

Methods for introducing a number of very pure gases, for heating the tip, for changing its orientation in space, and for cooling the tip below 60 K (in order to improve image resolution) introduce additional complexity. Currently, commercial field-ion microscopes are not produced, although at least one large manufacturer of vacuum equipment (Vacuum Generators, England) will assemble custom instruments on an individual basis.

7.3.7. Microchannel-Plate Image Intensification

A convenient way of providing internal image intensification in an FIM relies on the use of microchannel plates.[149] These devices were first employed in field-ion microscopes in 1969.[150] Today, microchannel plate image intensification is routinely used.

[148] M. Khoshnevisan and C. H. Stephan, *J. Phys. E* **6**, 10 (1973).

[149] M. Lampton, *Sci. Am.* **245**, 62 (November 1981).

[150] P. J. Turner, P. Cartwright, M. J. Southon, A. Van Oostrom, and B. W. Manley, *J. Phys. E.* **2**, 731 (1969).

A microchannel plate (or MCP) is composed of a myriad of glass capillaries arranged in an ordered array that is produced by selectively etching a fiber-optic bundle. The plate, which can have a diameter of many centimeters, is usually about 1.5 mm thick and can be planar or spherically curved. A planar MCP viewed normal to its surface in an optical microscope is shown in Fig. 20. The capillary tubes are typically less than 40 μm in diameter, and usually spaced on 50-μm centers. Each capillary acts as an individual electron multiplier when a potential difference of several hundred volts is applied across the conductive coatings that are deposited on each side of the MCP. Incoming ions (or electrons) that strike a capillary wall will produce, on the average, more than one secondary electron. These electrons are propagated through the channel by the electric field produced by the applied potential. Since the secondary electrons collide with the capillary wall several times during transit, an electron avalanche will result. One ion striking the entrance to a capillary can easily produce a thousand electrons at its end. By properly biasing the front surface of the MCP, particles that strike the intercapillary area between adjacent channels can be collected.[151] Although the efficiency of the MCP can approach 100% in this mode of operation, its spatial resolution will be correspondingly degraded.

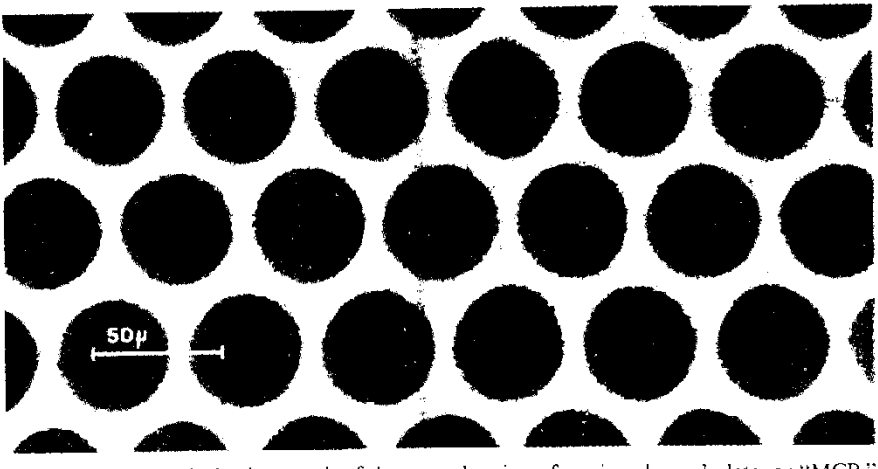

FIG. 20. An optical micrograph of the central region of a microchannel plate, or "MCP," which is also known as a CEMA (channel electron multiplier array). Each dark circular area is the entrance to a microcapillary tube that is typically 40 μm in diameter. A CEMA provides a convenient way to intensify a weak field-ion image. By combining two MCPs in tandem a gain of 10^6 can be achieved, which is sufficient to image single ions or electrons. (From Panitz.[27a] Copyright 1982 The Institute of Physics.)

[151] J. A. Panitz and J. A. Foesch, *Rev. Sci. Instrum.* **47**, 44 (1976).

The secondary electrons that emerge from each channel of an MCP are usually electrostatically focused onto a transparent phosphor-coated plate, where they produce a visible spot of light. If a field-ion image has sufficient magnification that the ions produced above adjacent surface species are separated at the MCP by several channel diameters, the entire weak field-ion pattern will be visible as a high-resolution image in ambient room light. By cascading two microchannel plates in tandem, a gain of 10^6 can be achieved. With MCP detectors, even the images resulting from individual field-desorbed ions can be recorded.[152]

The widespread use of a microchannel plate image intensification has greatly extended the utility of the field-ion microscope. Previously, many materials of interest could not be imaged because their lattice field evaporated before BIV was reached. With internal MCP detectors, materials that slowly field-evaporate during imaging can be photographed because exposure times less than a tenth of a second are usually adequate.

7.3.8. Surface Diffusion Studies Using the FIM

The ability of the field-ion microscope to observe individual metallic atoms adsorbed on atomically clean surfaces was recognized by Müller[153] as an important asset in performing surface diffusion experiments. The first quantitative measurements of diffusion parameters were made in 1966 when Ehrlich and Hudda[154] investigated the migration of tungsten atoms adsorbed on individual crystal planes of a tungsten tip. Later, Ehrlich and Kirk[155] field-desorbed tungsten adatoms from tungsten in order to obtain a binding energy for the metallic adsorbate. Other experiments followed that investigated the motion of individual adatoms,[156–160] adatom clusters and their dissociation,[161–163] pairs of adatoms cooperatively diffusing through a

[152] R. J. Walko and E. W. Müller, *Phys. Status Solidi, A* **9**, K9 (1972).
[153] E. W. Müller, *Z. Electrochem.* **61**, 43 (1957).
[154] G. Ehrlich and F. G. Hudda, *J. Chem. Phys.* **44**, 1039 (1966).
[155] G. Ehrlich and C. F. Kirk, *J. Chem. Phys.* **48**, 1465 (1968).
[156] E. W. Plummer and T. N. Rhodin, *J. Chem. Phys.* **49**, 3479 (1968).
[157] D. W. Bassett and M. J. Parsely, *J. Phys. D* **2**, 13 (1969).
[158] D. W. Bassett and M. J. Parsely, *J. Phys. D* **3**, 707 (1970).
[159] T. T. Tsong, *J. Chem. Phys.* **54**, 4205 (1971).
[160] P. G. Plative and W. R. Graham, *Thin Solid Films* **51**, 175 (1978).
[161] D. W. Bassett and M. J. Parsely, *Nature (London)* **221**, 1046 (1969).
[162] D. W. Bassett, *Surf. Sci.* **23**, 240 (1970).
[163] D. W. Bassett and D. R. Tice, *Surf. Sci.* **40**, 499 (1973).

long-range interaction,[164-173] and surface rearrangement with and without an electric field.[165,174,175]

The procedure for performing a diffusion experiment in the FIM is straightforward but tedious. Field evaporation is used to obtain a clean and atomically perfect surface that is then characterized by low-temperature field-ion microscopy. For adatom studies, a metallic adsorbate is deposited onto the tip in the absence of the field (usually by thermal evaporation from a heated filament). If field-ion imaging shows that the adsorbate coverage is too great, the field can be raised in order to remove some of the adsorbed species. Eventually, the desired number of adsorbates in the required lattice location will be obtained.

Surface diffusion is initiated by heating the tip to a known temperature (usually 200–500 K) for a fixed interval of time. Generally, the tip is not imaged during the diffusion interval in order to allow the diffusion process to occur in the absence of a field. Some measurements of diffusion in the presence of a field have been made. They yield information on the polarizability and the surface-induced dipole moment of an adatom.[176-179] Following the diffusion interval, the tip is cooled and a low-temperature field-ion image is taken of the new adatom position on the surface. The process is repeated, often hundreds of times. From a series of sequential field-ion images, the mean square displacement of an adatom over the surface can be measured as a function of diffusion temperature. A measurement accuracy of 0.01 nm is possible because adatom displacements can be directly compared to known interatomic spacings on well-resolved crystal planes in the FIM image.

A diffusion experiment will typically involve many temperature cycles and may last for many hours. As a result, ultrahigh-vacuum conditions and pressures below 10^{-10} Torr are mandatory if a contaminant-free surface is to

[164] T. T. Tsong, *J. Chem. Phys.* **55**, 4658 (1971).
[165] T. T. Tsong, *Phys. Rev. B* **6**, 417 (1972).
[166] W. R. Graham and G. Ehrlich, *Phys. Rev. Lett.* **31**, 1407 (1973).
[167] G. Ayrault and G. Ehrlich, *J. Chem. Phys.* **60**, 281 (1974).
[168] W. R. Graham and G. Ehrlich, *J. Phys. F.* **4**, L212 (1974).
[169] T. T. Tsong, P. Cowan, and G. Kellogg, *Thin Solid Films* **25**, 97 (1975).
[170] W. R. Graham and G. Ehrlich, *Thin Solid Films* **25**, 85 (1975).
[171] T. Sakata and S. Nakamura, *Surf. Sci.* **51**, 313 (1975).
[172] P. A. Reed and G. Ehrlich, *Philos. Mag.* **32**, 1095 (1975).
[173] K. Stolt, W. R. Graham, and G. Ehrlich, *J. Chem. Phys.* **65**, 3206 (1976).
[174] D. W. Bassett, *Surf. Sci.* **53**, 74 (1975).
[175] S. Nishigaki and S. Nakamura, *Jpn. J. Appl. Phys.* **15**, 19 (1976).
[176] T. T. Tsong and R. J. Walko, *Phys. Status Solidi, A* **12**, 111 (1972).
[177] W. R. Graham and G. Ehrlich, *Surf. Sci.* **45**, 530 (1974).
[178] T. T. Tsong and G. L. Kellogg, *Phys. Rev. B* **12**, 1343 (1975).
[179] G. L. Kellogg and T. T. Tsong, *Surf. Sci.* **62**, 343 (1977).

be preserved. The main difficulty that is encountered is the elimination of ambient hydrogen. The concentration of hydrogen will be increased in the vicinity of the tip during imaging by polarization forces and increased on the surface by field adsorption when the field is present.

The mean square displacement of an adatom $\langle x^2 \rangle$, measured in a diffusion experiment in a time interval γ, is related to the diffusion coefficient by the Einstein[180] equation

$$D = \langle x^2 \rangle / 2\alpha\gamma, \tag{7.3.6}$$

where D is the diffusion coefficient, and $\alpha = 1$ for the one-dimensional diffusion [viz., diffusion between two rows of atoms, e.g., diffusion on the (211) plane of tungsten]. For two-dimensional diffusion, $\alpha = 2$ and the one-dimensional displacement of Eq. (7.3.6) must be replaced with $\langle x^2 \rangle + \langle y^2 \rangle$. The mean square displacement can be related to the number of jumps N that the adatom experiences. For the one-dimensional case, random walk theory[181] predicts

$$\langle x^2 \rangle = NL^2, \tag{7.3.7}$$

where L is the mean jump distance. If a mean jump frequency Γ is defined as the number of adatom jumps per jump interval, the diffusion coefficient becomes

$$D = L^2\Gamma/2. \tag{7.3.8}$$

If we assume that diffusion occurs by thermal activation (with the adatom hopping from site to site across an atomically smooth surface), the mean jump frequency will be related to the activation energy for surface diffusion E_d by an expression of the form

$$\Gamma = \nu_0 \exp(-E_d/kT), \tag{7.3.9}$$

where k is Boltzmann's constant, T is the temperature, and ν is a pre-exponential frequency factor

$$\nu = \nu_0 \exp(\Delta S/K). \tag{7.3.10}$$

In Eq. (7.3.10), ΔS is the activation entropy and ν_0 is the atomic vibrational frequency. Although ν_0 is not known, its magnitude can be estimated from the uncertainty principle for energy and time. That is

$$\nu_0 = \Delta E/h \approx kT/h. \tag{7.3.11}$$

[180] A. Einstein, *Ann. Phys. (Leipzig)* **17**, 549 (1905); **19**, 371 (1906).

[181] See, e.g., W. Teller, "An Introduction to Probability Theory and Its Applications," 3rd Ed. Wiley, New York, 1967.

Experimental results are usually expressed in terms of the activation energy for surface diffusion E_d and the diffusivity D_0. The diffusivity is defined in terms of the diffusion coefficient. Combining Eqs. (7.3.8)–(7.3.11) yields

$$D = D_0 \exp(-E_d/kT), \tag{7.3.12}$$

where

$$D_0 \equiv \nu L^2/2 = (kTL^2/2h) \exp(\Delta S/k) \approx kTL^2/2h. \tag{7.3.13}$$

Since the activation entropy is usually negligible (at least for single-atom diffusion), the diffusivity at room temperature can be estimated by assuming a typical jump distance, say $L = 0.3$ nm. In this case, $D_0 = 3 \times 10^{-3}$ cm^2 s^{-1}.

To obtain a value for the diffusivity and the activation energy in terms of experimentally measurable parameters, Eqs. (7.3.6) and (7.3.12) are combined to give

$$\langle x^2 \rangle / 2\gamma = D_0 \exp(-E_d/kT). \tag{7.3.14}$$

If the mean square displacement of the adatom $\langle x^2 \rangle$ is measured in a time interval γ as a function of temperature, then an Arrhenius plot of $\langle x^2 \rangle/2$ versus $1/T$ will yield a straight line of slope $-E_d/k$ and intercept $\ln D_0$. Figure 21 shows a typical example in which individual tungsten adatoms and single diatomic tungsten clusters were diffused on the (110) plane of tungsten. Typical activation energies range from 0.16 eV for a rhodium adatom on Rh(111),[167] where $D_0 = 2 \times 10^{-4}$ eV, to 1.04 eV for a rhenium adatom on W(110),[157,158] where $D_0 = 1.5 \times 10^{-2}$. Diffusivities average about 0.3 cm^2 s^{-1}, which is typical for a rhodium adatom on Rh(110),[167] where $E_d = 0.6$ eV. More complete tabulations of the results of FIM diffusion experiments appear in excellent reviews by Kellogg *et al.*[182] and others.[183–187] A bibliography of FIM surface diffusion studies between 1951 and 1978 is included in a bibliography of field-ion microscopy and related techniques.[188]

[182] G. L. Kellogg, T. T. Tsong, and P. Cowan, *Surf. Sci.* **70**, 485 (1978).

[183] D. W. Bassett, *in* "Surface and Defect Properties of Solids" (M. W. Roberts and J. M. Thomas, eds.), Vol. 2, p. 34. Chem. Soc., London, 1973.

[184] G. Ehrlich, *Surf. Sci.* **63**, 422 (1977).

[185] M. W. Roberts and C. S. McKee, "Chemistry of the Metal–Gas Interface" Oxford Univ. Press (Clarendon), London and New York, 1978.

[186] T. T. Tsong and P. Cowan, *in* "Chemistry and Physics of Solid Surfaces" (R. Vanselow, ed.), Vol. 2, p. 209. CRC Press, Boca Raton, Florida, 1977.

[187] D. A. King, *J. Vac. Sci. Technol.* **17**, 241 (1980).

[188] R. E. Thurstans and J. M. Walls, "Field-Ion Microscopy and Related Techniques: A Bibliography 1951–1978," p. 123. Warwick, Birmingham, England, 1980.

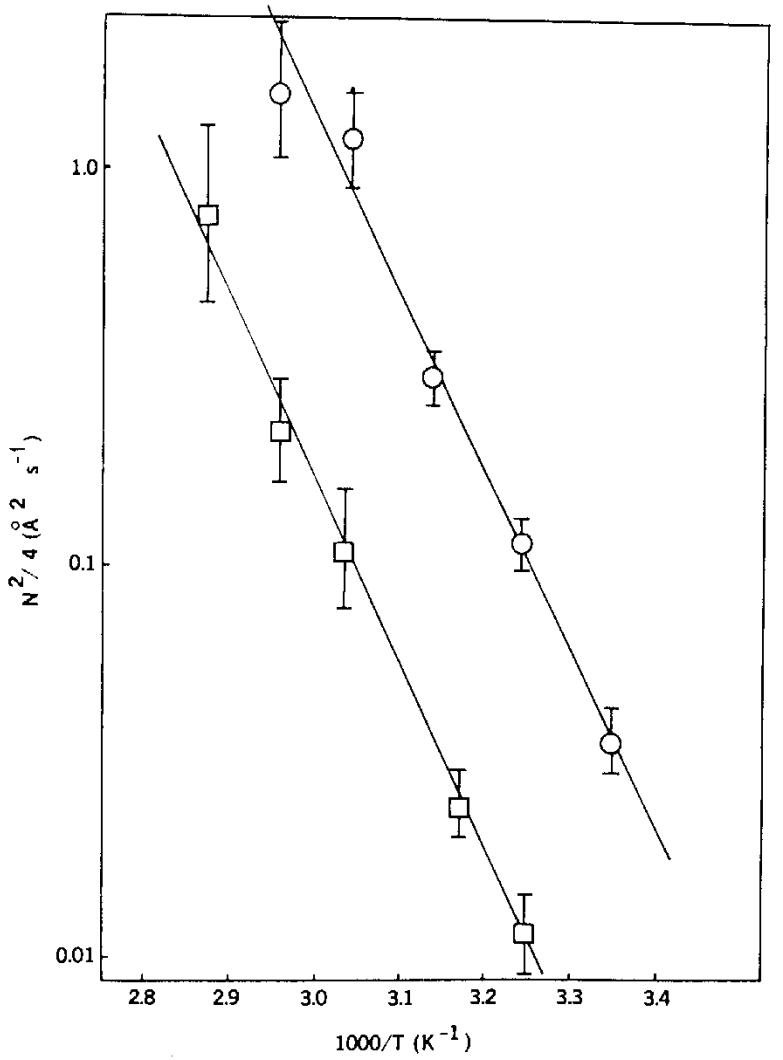

FIG. 21. Arrhenius plots for (○) single W adatom and (□) single W_2 cluster diffusion on the W(110) plane. From the plots the activation energy of surface diffusion is derived to be 0.90 ± 0.07 eV and 0.92 ± 0.14 eV for W and W_2, respectively. The diffusivity D_0 derived is 6.2×10^{-3} and 1.4×10^{-3} cm^2 s^{-1} for W and W_2, respectively. (Figure courtesy of Sandia National Laboratories, Albuquerque, New Mexico.)

7.4. Field Evaporation

At the present time there is no theory that accurately predicts all facets of the field evaporation phenomenon despite extensive discussions in the literature[129,189-197] and many excellent reviews.[28,126,198,199] Müller's original "image-force" theory of field evaporation described the process in terms of thermal activation over a field-reduced energy barrier. In this model, a neutral species is desorbed from the surface and then ionized at the critical distance given by Eq. (7.3.2). Despite its simplicity, the image-force theory predicts many of the experimental observations quite accurately.

In the image-force theory, a neutral species is removed from its surface site by supplying a sublimation energy Λ, which is assumed to be site independent. At the critical distance ionization occurs, which requires an additional energy $\Sigma_n I_n$ equal to the sum of ionization potential up to the nth value. Since the ion finds itself in an electric field, it can be polarized, which gives us an additional energy $(\alpha_a - \alpha_i)F^2/2$ where α_a and α_i are the polarizabilities of the neutral atom and the ion, respectively. But the tunneling electrons travel back to the metal, resulting in an energy gain of $n\Phi$, where Φ is a crystallographically dependent work function and n is the charge state of the ion. The total energy corresponding to all of these contributions can be considered as a binding energy Q, where

$$Q = \Lambda + \sum_n I_n - n\Phi - F^2(\alpha_a - \alpha_i)/2. \tag{7.4.1}$$

Although the last term of Eq. (7.5.1) can be a significant contribution to the total binding energy, it is usually ignored in the basic theory because the polarizability of the surface atom α_a is not reliably known.

In the presence of an applied field, the energy barrier represented by Eq. (7.4.1) is lowered by the amplitude of the so-called "Schottky hump." The magnitude of the effect can be found by considering the potential experienced by an ion of charge ne near the surface

$$V = -F(ne)x - (ne)^2/4x, \tag{7.4.2}$$

[189] R. J. Gomer, *J. Chem. Phys.* **31**, 341 (1959).
[190] E. W. Müller, *IV Int. Kongr. Elektronenmikrosk., Berlin, 1958*, **1**, 820 (1960).
[191] R. Gomer and L. W. Swanson, *J. Chem. Phys.* **38**, 1613 (1963).
[192] L. W. Swanson and R. Gomer, *J. Chem. Phys.* **29**, 2813 (1963).
[193] D. G. Brandon, *Br. J. Appl. Phys.* **14**, 474 (1963).
[194] D. G. Brandon, *Philos. Mag.* **14**, 803 (1966).
[195] T. T. Tsong, *Surf. Sci.* **10**, 102 (1968).
[196] T. T. Tsong and E. W. Müller, *Phys. Status Solidi A* **1**, 513 (1970).
[197] D. McKinstry, *Surf. Sci.* **29**, 37 (1972).
[198] D. G. Brandon, *Surf. Sci.* **3**, 1 (1965).
[199] E. W. Müller and T. T. Tsong, *Prog. Surf. Sci.* **4**, 11 (1973).

where the last term is the classical image potential mentioned previously in connection with the Fowler–Nordheim theory of field-electron emission. Once again, it should be stressed that a classically derived image potential is strictly incorrect, at least close to the surface where quantum effects will become dominant.

The amplitude of the Schottky hump is found by setting the derivative of Eq. (7.4.2) equal to zero. The result, $(n^3e^3F)^{1/2}$, reduces the energy barrier to desorption presented by the binding energy of Eq. (7.4.1). As a result, the activation energy for desorption is just

$$Q = \Lambda + \sum_n I_n - n\Phi - (n^3e^3F)^{1/2}. \tag{7.4.3}$$

Equation (7.4.3) specifically ignores the binding energy due to field-induced polarization. The characteristic time required for thermal activation over the barrier is of the form

$$\gamma = \gamma_0 \exp(-Q/kT), \tag{7.4.4}$$

where γ_0 is the reciprocal of the characteristic vibrational frequency of the atom bound to the surface at temperature T. The image-force theory predicts from Eqs. (7.4.3) and (7.4.4) a desorption field strength F_d given by

$$F_d = \left(\Lambda + \sum_n I_n - n\Phi - kT \ln \gamma/\gamma_0\right)^2 / n^3e^3. \tag{7.4.5}$$

At low temperatures, the last term in Eq. (7.4.3) is usually negligible, so that

$$F_d = \left(\Lambda + \sum_n I_n - n\Phi\right)^2 / n^3e^3. \tag{7.4.6}$$

For $n = 1$, the evaporation fields predicted by Eq. (7.4.6) differ significantly from those observed experimentally for most metals. However, when doubly charged ions are assumed, the agreement with experiment is reasonably good. Brandon[198] found that the calculated evaporation field for most metals was a minimum for $n = 2$, suggesting that most metals should evaporate as a doubly charged ion. An identical result is obtained from Gomer and Swanson's more detailed treatment of the field-desorption process.[192] They predict an evaporation field

$$F_d = (\Lambda + I_n - n\Phi - n^2e^2/X_c)/ne_c, \tag{7.4.7}$$

where X_c is the critical distance for ionization. In practice, X_c is assumed to be equal to the single-bond atomic radius of the metal atom.

Mass spectrometric measurements of iron and nickel made by Barofsky

and Müller[200,201] supported the general conclusion of an $n = 2$ species, but for other materials the charge state of the field-evaporated ion depended critically on the emitter temperature. For example, beryllium was shown to evaporate exclusively as Be^{2+} at 21 K. However, at the same ion flux, Be^{+} appeared as the emitter temperature was raised, and increased in abundance to become the dominant species at room temperature. As the temperature of the emitter is increased, the electric field strength required to maintain a constant ion flux (or field-evaporation rate), decreases. Therefore, by changing the emitter temperature, one actually measures the relative charge-state abundances as a function of both the electric field strength and the temperature. Ernst[202] has suggested that a decrease in the abundance of Rh^{2+} ions with decreasing field strength and increasing temperature is due to post-ionization Rh^{+} desorbed from the surface. In the post-ionization model, a species is assumed to leave the tip surface in a low charge state. Higher charge states are acquired by subsequent ionization in space. One or more electrons are lost to the metal by tunneling as the ion moves rapidly away from the tip. The process is strongly dependent on the electric field strength and may also depend on the local crystallography of the surface. By using a one-dimensional tunneling probability, Ernst was able to predict the relative abundance of singly and doubly charged rhodium ions as a function of field strength to within a factor of two.[202] A more refined, three-dimensional calculation by Haydock and Kingman[203] strongly supports the post-ionization model. Haydock and Kingman suggest that multiple post-ionizations may be responsible for the higher charge states of molybdenum and tungsten that are observed experimentally. This conclusion is supported by a study in which Kellogg[204,205] observed a charge-state abundance for a number of materials, over a wide field range, that agreed with Haydock and Kingman's predictions. Post-ionization appears to be the dominant mechanism for producing the higher charge states of field-evaporated metal ions.

7.5. Field-Ion Mass Spectroscopy

In addition to providing valuable insight into the physical mechanisms responsible for the ionization event, ions produced by a high electric field can be used in an analytical capacity to determine the composition of un-

[200] P. F. Barofsky and E. W. Müller, *Surf. Sci.* **10**, 177 (1968).
[201] D. F. Barofsky and E. W. Müller, *Int. J. Mass Spectrom. Ion Phys.* **2**, 125 (1969).
[202] N. Ernst, *Surf. Sci.* **87**, 469 (1979).
[203] R. Haydock and D. R. Kingman, *Phys. Rev. Lett.* **44**, 1520 (1980).
[204] G. L. Kellogg, *Phys. Rev. B* **24**, 1848 (1981).
[205] G. L. Kellogg, *Surf. Sci.* **120**, 319 (1982).

known samples. Field-ionization mass spectroscopy began modestly in 1954 when Inghram and Gomer[125] published the first quantitative study of field-ionized hydrogen, nitrogen, oxygen, methyl alcohol, and hydrocarbon species. Later, they were able to demonstrate that some species (such as CH_3O^+ in the spectrum of methyl alcohol) did not originate in the gas phase but were produced at the tip surface and supplied by continuous migration of a condensed phase on the tip shank.[206]

One advantage of using high electric fields to induce ionization lies in the ionization process itself. Ionization in an electric field produces a fragmentation pattern different from (and often simpler than) a conventional electron-bombardment ionization source.[207,208] As a result, a gas-phase spectrum taken with a combined electron-bombardment and field-ionization source[209-212] can provide more information than either source alone and is often easier to interpret. Since vibrational or electronic excitations are not generally induced under high-field conditions, metastable complexes can often be identified in the field-ionization mass spectra. Unfortunately, these advantages can be offset by a complex field-induced chemistry,[207] whose interpretation may require a detailed knowledge of the ion formation mechanism.[207,213] Systematic application of field desorption mass spectrometry to a wide range of practical problems, including medical diagnosis,[214-217] coal research,[218] drug[219] and environmental pollutant detection,[216,220,221] and problems of catalysis,[222,223] have established the technique as a useful molec-

[206] M. G. Inghram and R. Gomer, *Z. Naturforsch. A* **10A,** 863 (1955).
[207] H. D. Beckey, "Field Ionization Mass Spectrometry." Pergamon, Oxford, 1971.
[208] H. R. Schulten and H. D. Beckey, *Tetrahedron* **29,** 3861 (1973).
[209] H. H. Gierlich, A. Heindric, and H. D. Beckey, *Rev. Sci. Instrum.* **45,** 1208 (1974).
[210] M. Anbar and G. A. St. John, *Anal. Chem.* **48,** 198 (1976).
[211] H. R. Schulten and N. M. M. Nibbering, *Biomed. Mass Spectrom.* **4,** 55 (1977).
[212] A. M. Hogg and J. D. Payzant, *Int. J. Mass Spectrom. Ion Phys.* **27,** 291 (1978).
[213] F. W. Rollgen, V. Giessmann, H. J. Heinen, and H. D. Beckey, *Ultramicroscopy* **4,** 375 (1979).
[214] H. R. Schulten, W. D. Lehmann, and Z. Ziskoven, *Z. Naturforsch., C* **33C,** 484 (1978).
[215] H. Miyazaki, E. Shirai, M. Ishibashi, K. Hosoi, S. Shibata, and M. Iwanaga, *Biomed. Mass Spectrom.* **5,** 559 (1978).
[216] H. R. Schulten, *Int. J. Mass Spectrom. Ion Phys.* **32,** 97 (1979).
[217] H. R. Schulten and D. Kummler, *Anal. Chim. Acta* **113,** 253 (1980).
[218] T. Yoshida, R. Yoshida, Y. Maekawa, Y. Yoshida, and Y. Itagaki, *Fuel* **58,** 153 (1979).
[219] D. A. Brent, *J. Assoc. Off. Anal. Chem.* **59,** 1009 (1976).
[220] H. R. Schulten, *J. Agric. Food Chem.* **24,** 743 (1976).
[221] Y. Yamato, M. Suzuki, and T. Watanabe, *Biomed. Mass Spectrom.* **6,** 205 (1979).
[222] W. A. Schmidt, O. Frank, and A. W. Czanderna, *Phys. Status Solidi A* **16,** 127 (1973).
[223] W. A. Schmidt, O. Frank, and J. H. Bloch, *Surf. Sci.* **44,** 185 (1974).

ular probe. Several excellent reviews[224-229] summarize advances in this rapidly expanding area.

7.5.1. Field-Ionization Sources

A gas-phase field-ionization source is unique in that it can supply a reasonably monoenergetic beam of positive ions that appear to originate from a point in space when a single emitter tip is used. If an extended ionization region can be used, multiple tip structures, produced by microfabrication techniques,[230] grown on filaments of platinum or carbon, or occurring naturally on extended metal edges (such as razor blades), can be employed.[207] Their advantage lies in their large surface area and the correspondingly high ion currents that they are capable of generating.

The nearly monoenergetic nature of the ions produced by the field-ionization process is illustrated by the 0.8 eV FWHM helium-ion energy distribution at BIV above a single emitter tip, as shown in Fig. 14. Monoenergetic ions, like monochromatic light, can be focused to a small diameter spot because chromatic aberration will be absent from the image. The ability to focus the ions from a field-ion source is important, not only in mass spectroscopy but also in other applications. For example, if a field-ion beam can be focused to submicron dimensions, it can be used as a microanalytical probe[231] or as a tool to fabricate submicron structures by direct ion sputtering.

In order to estimate the ion current produced by a single emitter tip, the apex of the tip can be treated as a sphere of radius R. In this case, the surface area of the tip apex that actually contributes to the ionization process will be $2R^2\theta$, where θ defines the angle in radians over which field ionization can occur. Since the electric field strength at the surface of a tip decreases with increasing angle from the apex,[21] there will be a maximum angle beyond which field ionization will not occur. Experimentally, $\theta_{max} \approx \pi/4$, so that the total surface area of a field emitter that contributes to the ionization current will be of the order of πR^2. If we assume that 10^5 ions s^{-1} are produced over

[224] H. D. Beckey, *Res./Dev.* **20**, 26 (1969).
[225] J. A. B. Robertson, *J. Phys. E* **7**, 321 (1974).
[226] P. J. Derrick, *Mass Spectrom.* **4**, 132 (1977).
[227] H. D. Beckey, K. Levsen, F. W. Rollgen, and H. R. Schulten, *Surf. Sci.* **70**, 325 (1978).
[228] D. L. Cocke and J. H. Bloch, *Surf. Sci.* **70**, 363 (1978).
[229] W. D. Reynolds, *Anal. Chem.* **51**, 283A (1979).
[230] C. A. Spindt, I. Brodie, L. Humphrey, and E. R. Westerberg, *J. Appl. Phys.* **47**, 5248 (1976).
[231] G. R. Hansen and B. M. Siegel, *J. Vac. Sci. Technol.* **16**, 1875 (1979).

each surface atom in this region, a typical field-ion source (with $R = 100$ nm) will produce a total field-ion current of 10^{11} ions s^{-1}, or about 10 nA.

One difficulty in developing such a source lies in focusing the entire ion beam, which diverges into a solid angle of approximately π sr. A typical lens system will accept ions within a solid angle of perhaps $\pi/10$ sr, so that the usable current from a field-ion source may be only of the order of a few nanoamperes. Another difficulty results from the variation of the field-ion current with time. Variations in the source current will appear as a low-frequency "flicker noise" in the focused spot. Orloff and Swanson[232] have developed low-noise field ionization sources with angular current densities approaching 10 μA sr^{-1}. Hansen and Siegel[231] have shown that 60 μA sr^{-1} can be achieved by field-desorbing hydrogen physisorbed on tungsten at liquid-helium temperatures. Their source uses ions that originate at one of the stable, localized, and anomalously bright regions that were previously observed in hydrogen field-ion images of tungsten at 4.2 K.[233] By using a variety of gases, Hansen and Siegel hope to increase the versatility of such a source. They propose to create and focus a beam of light ions (such as H_2^+ or He^+) in order to expose patterns on a semiconductor surface coated with a suitable resist. Heavier ions, such as Ar^+ and Xe^+, would be used to sputter such patterns directly into the surface.

7.5.2. Liquid-Metal Field Desorption Sources

The production of a focused beam of metallic species could be used to selectively dope small regions of a semiconductor surface by ion implantation or as a probe in a scanning ion microscope. One way to produce a continuous beam of metallic ions is to place a supply of weakly bound metallic adatoms on the surface of a tip biased to high voltage. If the adatoms were mobile on the surface, polarization forces would draw them into the high-field region of the tip apex where field desorption would occur. Since most metals are not mobile at room temperature, such a scheme would require heating the tip to an elevated temperature. A continuously operating source would also require a reservoir of metal atoms to replenish those lost by the desorption process.

Krohn and Ringo[234] investigated such a source and measured ion currents of several microamperes. The ion current persisted as long as a thick layer of liquid metal was present on the tip surface. The half-width of a typical energy distribution was found to be ~ 12 eV FWHM, a value later measured with

[232] J. H. Orloff and L. W. Swanson, *J. Vac. Sci. Technol.* **12**, 1209 (1975); **15**, 845 (1978); *J. Appl. Phys.* **50**, 6026 (1969).

[233] A. Jason, B. Halpern, M. G. Inghram, and R. Gomer, *J. Chem. Phys.* **52**, 2227 (1970).

[234] V. E. Krohn and G. R. Ringo, *Appl. Phys. Lett.* **27**, 479 (1975).

greater precision by Culbertson *et al.*[235] for a gallium source. At very low currents (of the order of 10 nA) Culbertson and co-workers[235] found that the Ga^+ energy distribution sharpened to ~ 1.5 eV FWHM. This suggested that under conditions of low emission the ionization process was occurring within a thin layer of gallium atoms on the surface.

The metallic layer on the tip surface appears to form a stable, pointed protrusion at the tip apex in the presence of a field. This protrusion is responsible for the ion current that is observed. It is called a "Taylor cone," and is created by a balance of electrostatic and surface tension forces at the surface of the molten metal. The cone behaves as though it were a continuously field-evaporating tip. In 1964, Sir George Taylor[236] showed that a cone of half-angle 49.3° will be produced at the surface of a liquid under the influence of a critical electric field strength that depends on the geometry of the source. In principle, a Taylor cone, once created, is dynamically stable and infinitely sharp. In practice, instabilities can occur that may lead to the formation of a liquid jet or a stream of isolated droplets. A liquid-metal field-ion source can produce a single or multiple Taylor cone structure on the tip apex. Electron microscope images of an operating source have been obtained, but the resolution is not sufficient to show the shape of each structure in detail. Gomer[237] has presented a comprehensive theoretical treatment of liquid-metal sources. Experimental sources have been constructed using a variety of liquid metals. These include gallium,[234,238] the alkali metals,[235,239,240] gold,[241] alloys such as Wood's metal,[242] and mercury.[241] A focused liquid-gallium source capable of producing submicron gallium structures has been described by Seliger.[243] Levi-Setti[244] has shown that a liquid-gallium source can be used to produce scanning ion micrographs with excellent resolution. Waugh[245] has shown that elemental mapping of surface composition can be achieved by using a liquid-gallium source for secondary-ion mass spectroscopy (SIMS).

[235] R. J. Culbertson, T. Sakurai, and G. H. Robertson, *J. Vac. Sci. Technol.* **16,** 574 (1979).

[236] G. I. Taylor, *Proc. R. Soc. London, Ser. A* **280,** 383 (1964).

[237] R. Gomer, *J. Appl. Phys.* **19,** 365 (1979).

[238] T. Sakurai, R. J. Culbertson, and J. H. Robertson, *Appl. Phys. Lett.* **34,** 11 (1979).

[239] J. F. Mahoney, A. T. Yahiku, H. L. Daley, R. D. Moore, and J. Perel, *J. Appl. Phys.* **40,** 5101 (1969).

[240] R. Clampitt, K. L. Aitken, and D. K. Jefferies, *J. Vac. Sci. Technol.* **12,** 1208 (1975).

[241] R. Clampitt and D. K. Jefferies, *Nucl. Instrum. Methods* **149,** 739 (1978).

[242] B. W. Colby and C. A. Evans, Jr., *Anal. Chem.* **45,** 1887 (1973).

[243] R. D. Seliger, *Ultramicroscopy* **4,** 361 (1979).

[244] R. Levi-Setti, P. H. LaMarche, and K. Lam, *Proc. Int. Field-Emiss. Symp., 29th, Göteborg, Sweden,* p. 417, H. Nordén and H. O. Andren, eds. (Almquist and Wiksell, Stockholm, 1982).

[245] A. R. Waugh, *Proc. Int. Field-Emiss. Symp., 29th, Göteborg, Sweden,* p. 409. H. Nordén and H. O. Andren, eds. (Almquist and Wiskell, Stockholm, 1982).

7.6. Atom-Probe Mass Spectroscopy

Barofsky and Müller's early measurements[192,193] suggested that a unique microanalytic capability could be provided by a mass spectrometer capable of identifying a small number of field-evaporating lattice constituents. In 1967, Müller and Panitz[246] proposed to make the entrance aperture of a spectrometer equal in area to a single magnified image spot in a field-ion micrograph. In this way they hoped to provide an ultimate microanalytic capability: the unambiguous identification of a single field-evaporated surface species. A magnetic sector spectrometer can be used for analysis, but it is not ideal since only a limited mass range can be observed at one time. If the mass-to-charge ratio of a single field-evaporated species fell outside of the preselected mass interval, it would not be detected. In order to overcome this difficulty, Barofsky[247] suggested the use of a time-of-flight (TOF) mass spectrometer. Such a spectrometer is simple to construct, has a wide mass range, and easily discriminates between a field-evaporated species and a random event. As a result, the TOF atom-probe is the most common form of this instrument in use today. Although many atom-probes are in use throughout the world, a commercial instrument is not currently available.

7.6.1. The Voltage-Pulsed Atom-Probe

The atom-probe[248] was named by analogy with the electron microprobe developed previously by Castaing.[249] Castaing's instrument could identify the constituents of a small macroscopic region of a sample containing perhaps 10^{11} atoms. With the atom-probe one could, in principle, "determine the nature of one single atom seen on a metal surface and selected from neighboring atoms at the discretion of the observer."[248] In order to achieve this goal, the field-ion image of a surface species is positioned over the entrance aperture of the time-of-flight mass spectrometer. This is accomplished by mechanically moving the tip assembly. Field evaporation is initiated by applying a short-duration high-voltage pulse to the tip. If the pulse amplitude is carefully adjusted, a few atoms of the surface layer or many layers of the near surface region, can be controllably removed.

On application of the high-voltage pulse, surface species are ionized and acquire a kinetic energy

$$mv^2/2 = neV_0, \tag{7.6.1}$$

[246] E. W. Müller and J. A. Panitz, *Abstr. 14th Int. Field-Emiss. Symp., Washington, D.C.* (1967). Unpublished.

[247] J. A. Panitz, *J. Phys. E.* **15,** 1281 (1982).

[248] E. W. Müller, J. A. Panitz, and S. B. McClane, *Rev. Sci. Instrum.* **39,** 83 (1968).

[249] R. Castaing, *Adv. Electron. Electron Phys.* **13,** 317 (1960).

where ne is the ion's charge and V_0 is the tip potential produced by the pulse. It is usually convenient to apply a dc bias to the tip so that $V_0 = V_{dc} + V_{pulse}$. To ensure adequate mass resolution, the high-voltage pulse must be sufficiently short so that the field-evaporation interval is much shorter than the arrival time at the detector of two neighboring species that are to be separated. A fixed point on the leading edge of the pulse can be used as a marker to identify the instant of time corresponding to the field desorption event. If we use this as the "zero" of time, the ion's travel time to a detector can be accurately measured.

The field-evaporated ions will acquire their full kinetic energy within a few tip radii from the surface. In order to define the acceleration region very precisely, a grounded plate containing an aperture is placed very close to the tip. The pulse duration must be sufficiently long to ensure that the ions have left this region before the pulse terminates. After the ions traverse the aperture, they enter a field-free "drift" region of length D. At some point within the drift region the ions encounter a fluorescent screen or MCP detector of the field-ion microscope. The screen or MCP contains a probe hole. Only the surface species whose image was positioned over the probe hole will continue to travel at constant velocity to a detector positioned at the end of the drift region. If T is the travel time of the ion measured from the instant of desorption, its mass-to-charge ratio will be given by Eq. (7.1.9). If m/n is expressed in atomic mass units, $V_{dc} + V_{pulse}$ is measured in kilovolts, the travel time is measured in microseconds, and the length of the drift region is measured in meters, Eq. (7.1.9) becomes

$$m/n = 0.193(V_{dc} + V_{pulse})T^2/D^2. \tag{7.6.2}$$

A typical mass resolution of $\Delta m/n \approx 1\%$ can be routinely achieved with the TOF atom-probe.[250] The mass resolution is limited primarily by a spread in the kinetic energy of the field-evaporating ions. This quantity can easily approach several hundred electron volts. The energy spread results from field evaporation during the time that the high-voltage pulse is changing in amplitude.[251,252] In order to improve the mass resolution, Müller and Krishnaswamy[253] used isochronal focusing to electrostatically compensate for the initial energy spread of the field-evaporated ions. An energy resolution of $\sim 0.1\%$ was achieved but at the expense of detection efficiency and instrumental simplicity. Another way to achieve high mass resolution is to use a magnetic-sector spectrometer. In this case, field desorption is continuous and produced by a dc bias applied to the tip. The resulting ions have a

[250] J. A. Panitz, *Prog. Surf. Sci.* **8**, 219 (1978).
[251] E. W. Müller, *Lab. Pract.* **22**, 408 (1973).
[252] S. V. Krishnaswamy and E. W. Müller, *Rev. Sci. Instrum.* **45**, 1049 (1974).
[253] E. W. Müller and S. V. Krishnaswamy, *Rev. Sci. Instrum.* **45**, 1053 (1974).

constant energy. A magnetic sector atom probe was constructed by Müller and Sakurai[254] in 1974. Another type of atom-probe, the *pulsed-laser atom-probe*, was suggested by Tsong[255] in 1978.

7.6.2. The Pulsed-Laser Atom-Probe

Field desorption is a thermally activated process. Tsong reasoned that a short-duration thermal pulse from a laser could be used instead of a voltage pulse to initiate field evaporation in a TOF spectrometer. Since the tip could be kept at a constant dc potential, the energy spread of the resulting ions should be of the order of kT, or less than 0.1 eV. An additional benefit of laser-induced desorption was foreseen. It is difficult to use the voltage pulsed atom-probe to examine insulators or high-purity semiconductors because of their high intrinsic resistance. The resistance of the tip and the capacitance between tip and ground form a low-pass filter. To propagate a pulse to the tip apex the pulse must have duration much greater than the time constant of the system. Any material with an intrinsic resistance of $10^8\ \Omega$ will produce a time constant of the order of milliseconds. This means that very long ion travel times (or very low tip voltages) would have to be used to assure good mass resolution in a TOF instrument. Since a high voltage must be applied to establish the desorption field, the ions would have to be decelerated. Focusing then becomes a problem. On the other hand, a tip can be easily pulsed to a high temperature with a laser. The pulse can be made several nanoseconds or less in duration, and a constant tip potential can be used. Furthermore, since field and temperature can be varied, the electric field strength applied to the tip can be reduced by using higher laser powers to establish a given evaporation rate. This would reduce the possibility of producing field-induced artifacts, or allow the production of such artifacts to be studied as a function of field strength. Since the surface temperature can be arbitrarily elevated during the desorption event, the effect of surface mobility can also be studied.

The feasibility of using a laser to thermally induce field evaporation in a TOF atom probe has been demonstrated by Kellogg and Tsong[256] and Drachsel *et al.*[257] The latter group believes they have also seen photon-induced (nonthermal) desorption during an examination of ethylene on silver.[258] Kellogg[259] has shown that the H^+ species normally observed in the

[254] E. W. Müller and T. Sakurai, *J. Vac. Sci. Technol.* **11**, 878 (1974).
[255] T. T. Tsong, *Surf. Sci.* **70**, 211 (1978).
[256] G. L. Kellogg and T. T. Tsong, *J. Appl. Phys.* **51**, 1184 (1980).
[257] W. Drachsel, S. Nishigaki, and J. H. Block, *Int. J. Mass Spectrom. Ion Phys.* **32**, 333 (1980).
[258] S. Nishigaki, W. Drachsel, and J. H. Block, *Surf. Sci.* **87**, 389 (1979).
[259] G. L. Kellogg, *J. Chem. Phys.* **74**, 1479 (1981).

voltage-pulsed atom-probe is an artifact, caused by field dissociation of adsorbed molecular hydrogen in the high electric field above the tip surface. He also demonstrated that silicon could be examined by atom-probe mass spectroscopy. Measurements by Tsong[260] have shown that the pulsed-laser atom-probe can achieve excellent mass resolution. However, the thermal response of the tip may actually be much slower than the duration of the laser pulse. Since desorption will be governed by the entire thermal cycling of the tip, its thermal time constant will ultimately determine the highest mass resolution that can be achieved.

7.6.3. Atom-Probe Measurements

Essentially three different measurements can be made with an atom-probe. Although spectra are recorded, the three measurements differ in procedure and ultimate aim. The first type of measurement is concerned with determining the relative abundances of species that reside *on* the first atomic layer of the specimen lattice. Since this layer will primarily consist of weakly bound residual gas species, desorption of this layer must be achieved without disturbing the underlying substrate lattice.

The second type of measurement is concerned with determining the relative abundance of species contained within each individual atomic layer of the substrate lattice. By field-evaporating the lattice one layer at a time and recording the abundance of all species within each layer, a depth profile of the near-surface region can be obtained.

The third type of measurement is concerned with determining an average composition for the near-surface region of the lattice. In this case, the abundance of each species is averaged over many atomic layers.

7.6.4. First-Layer Composition

In the absence of an electric field, species characteristic of the ambient environment will be adsorbed on the tip surface with a probability that will depend on their partial pressure in the gas phase, their abundance on the surface, and the temperature of the tip. In addition, weakly bound displaced lattice atoms may be present. At equilibrium, each of these species will exist on the surface at a unique position fixed by chemical or stearic interactions with the lattice. In a very real sense, the first layer of the tip surface is a microcosm of the ambient environment and the reaction of the tip material to it.

In order to determine the composition of the first layer, one assumes that the most tightly bound species of the first layer will desorb at a field strength

[260] T. T. Tsong, *Rev. Sci. Instrum.* **53**, 1442 (1982).

that is less than that necessary to field-evaporate the underlying lattice. In the case of strong chemical interactions with lattice atoms (as in chemisorption, or on the formation of chemical compounds) this assumption may fail. Experimentally, one tests the validity of this assumption by observing changes in a field-ion image of the lattice before and after desorption. Since the species that characterize the first layer will generally be more weakly bound than those of the bulk, they will be desorbed at field strengths that are well below the evaporation field of the lattice. Therefore, the analysis of the "first layer" begins by applying a very low field (typically less than 10 V nm^{-1}) where the probability of removing any species from the surface is known (from experience) to be vanishingly small. A mass spectrum is recorded at this field, and the tip bias (V_{dc}) is incremented by 50–100 V. Using a small increment in specimen bias increases the probability that, during the next pulse, species will be desorbed very close to the maximum amplitude of the desorption pulse. This, in turn, assures a minimum energy spread in the ions being desorbed and a maximum mass resolution for each spectrum recorded.

For each increment in tip bias a mass spectrum is recorded until a tip bias V_m is reached that is 50–100 V less than the lattice. It is assumed that at this point all species that resided on the first layer of lattice atoms have been desorbed. The composition of the first layer is obtained by summing the abundances that were recorded in the individual mass spectra during each desorption event.

Alternatively, the abundance of a species can be obtained as a function of desorption field. Crudely speaking, this is a measure of the binding of a species to the surface if the evaporation field for the lattice F_E and the corresponding evaporation bias V_E are known; the desorption field F, at specimen potential V can be calculated from the expression

$$F = (V/V_E)F_E. \tag{7.6.3}$$

By linearly increasing the tip potential with time and recording the total ion current, an analog to thermal-desorption mass spectrometry can be obtained.[261] Since the tip is kept at low temperature, thermal migration over the surface is eliminated, but field-induced migration remains a serious concern.

7.6.5. Composition of One Atomic Layer

The composition of a single atomic layer of the lattice as sampled by the probe hole can be obtained by summing the abundance obtained for each species recorded during the successive evaporation events required to remove the layer. It is assumed that all species that are contained within the

[261] J. A. Panitz, *J. Vac. Sci. Technol.* **16**, 868 (1979).

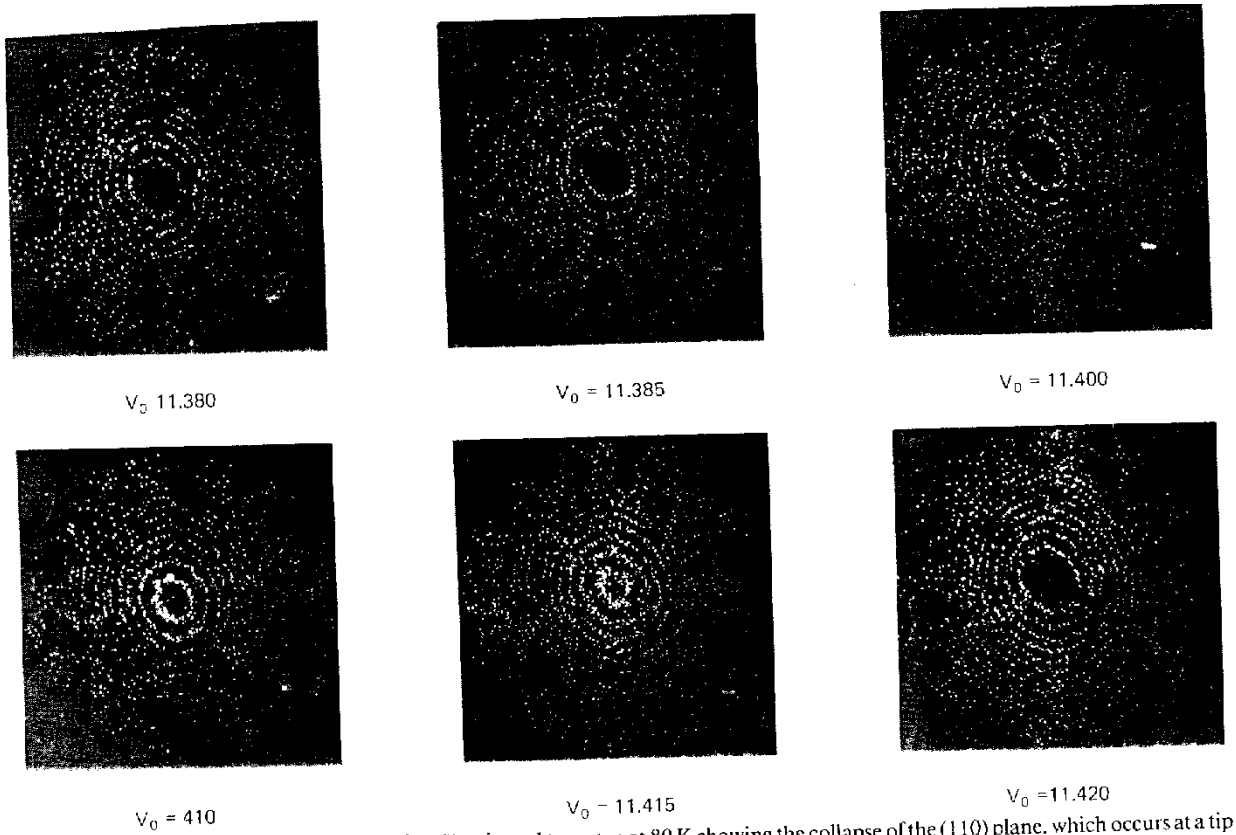

FIG. 22. A sequence of field-desorption images of (110)-oriented tungsten at 80 K showing the collapse of the (110) plane, which occurs at a tip bias $V_0 = 11.415$ V. $p \cong 5 \times 10^{-9}$ Torr. (From Panitz.[250])

layer are removed as positive ions and detected with the same efficiency. For a refractory metal substrate containing easily ionized low-Z impurities, the high field strength required to evaporate the lattice will probably guarantee the ionization of all species within the layer. For low-Z substrates containing high-Z impurities, the situation is less certain. Field evaporation will guarantee the removal of all species as the lattice dissolves, but the low field strength may not be sufficient to ensure complete ionization of all high-Z impurities. Since little is known about the ionization efficiency in high fields, the possibility of selective ionization cannot be ignored. Furthermore, since the single-ion detectors used in atom-probe devices are not particularly sensitive to low-energy neutrals, these species will go undetected. Only when all species are ionized with the same efficiency will the measured composition of each atomic layer accurately reflect its composition prior to desorption.

The removal of one atomic layer of the specimen is monitored by observing the collapse of a prominent net plane in the field-ion image of the lattice as shown in Fig. 22. If the layer spacing is known, the depth to which the lattice is probed will be uniquely determined. This "built-in" depth scale makes depth profiling with the atom probe as accurate as the known interplanar spacings of the lattice.

Unlike sputter-depth profiling, field evaporation will completely remove a monolayer without the possibility of driving some species of that layer further into the lattice or mixing species within the sampled region.[262] As a result, the atom probe is a unique tool that can characterize the depth distribution of low-energy species in metals,[147,263] and can be used as the basis of an extensive program of material characterization.[247–287] As a metallurgical tool, the unique spatial and depth resolution of the atom-probe provides a unique complement to existing microanalytic techniques. Numerous reviews[250,288–294] clearly demonstrate the growing importance of atom-probe analysis in the materials sciences.

[262] Z. L. Liau, B. Y. Tsaur, and J. W. Mayer, *J. Vac. Sci. Technol.* **16**, 121 (1979).
[263] A. Wagner and D. N. Seidman, *Phys. Rev. Lett.* **42**, 515 (1979).
[264] D. N. Seidman, *Proc. Microsc. Soc. Can.* **3**, 36 (1976).
[265] T. M. Hall, A. Wagner, A. S. Berger, and D. N. Seidman, *Metallography* **10**, 485 (1976).
[266] Y. S. Ng, S. B. McLane, and T. T. Tsong, *J. Appl. Phys.* **49**, 2517 (1978).
[267] M. K. Miller and G. D. Smith, *Met. Sci.* **11**, 249 (1977).
[268] D. N. Seidman, *Surf. Sci.* **70**, 532 (1978).
[269] S. Nakamura and T. Kuroda, *Surf. Sci.* **70**, 452 (1978).
[270] A. J. Watts and B. Ralph, *Surf. Sci.* **70**, 459 (1978).
[271] Y. Ohno, T. Kuroda, and S. Nakamura, *Surf. Sci.* **75**, 689 (1978).
[272] M. K. Miller, P. A. Beaven, R. J. Lewis, and G. D. W. Smith, *Surf. Sci.* **70**, 470 (1978).
[273] T. T. Tsong, Y. Ng, and S. V. Krishnawwamy, *Appl. Phys. Lett.* **32**, 778 (1978).
[274] A. Wagner, T. M. Hall, and D. N. Seidman, *J. Nucl. Mater.* **69**, 413 (1978).

7.6.6. Average Composition of the Near-Surface Region

By measuring the abundance of all species in each atomic layer, and summing over many layers, an average composition of a volume of the near-surface region is obtained. Since the tip potential must be increased as the lattiee is evaporated (to maintain a constant evaporation field as the tip radius increases), the travel times of a given species will become progressively shorter.

Unlike Auger spectroscopy, electron spectroscopy for chemical analysis (ESCA), or photoemission, the atom-probe technique is truly an invasive probe of the surface. The surface must be completely destroyed in order to identify its constituents. This means that any phenomenon that occurs on the surface can be sampled only once during its evolution. In order to extend the number of observations for statistical reliability (or to examine a phenomenon at a different point in its evolution) an identical surface must be recreated many times. If field-ion microscopy can be used to image the tip, and if field evaporation can be employed to reestablish an identical surface morphology, then reestablishing the phenomenon will be a question only of patience.

---

[275] T. T. Tsong, Y. S. Ng, and A. J. Melmed, *Surf. Sci.* **77,** L187 (1978).
[276] Y. S. Ng and T. T. Tsong, *Surf. Sci.* **78,** 419 (1979).
[277] Y. S. Ng, T. T. Tsong, and S. B. McLane, *Surf. Sci.* **84,** 31 (1979).
[278] G. K. L. Cranstoun, D. R. Pyke, and G. D. W. Smith, *Appl. Surf. Sci.* **2,** 375 (1979).
[279] S. Nakamura, Y. S. Ng, T. T. Tsong, and S. B. McLane, *Surf. Sci.* **87,** 656 (1979).
[280] S. V. Krishnaswmay, R. Messier, Y. S. Ng, and T. T. Tsong, *Appl. Phys. Lett.* **35,** 870 (1979).
[281] D. M. Seidman, *J. Met.* **31,** 116 (1979).
[282] P. A. Beaven, K. M. Delargy, M. K. Miller, P. R. Williams, and G. D. W. Smith, *Ultramicroscopy* **4,** 385 (1979).
[283] M. Leisch, *Ultramicroscopy* **4,** 381 (1979).
[284] S. V. Krishnaswamy, R. Messier, Y. S. Ng, T. T. Tsong, and S. B. McLane, *J. Non-Cryst. Solids* **35,** 351 (1980).
[285] P. W. Bach, J. Beyer, and C. A. Verbraak, *Scr. Metall.* **14,** 205 (1980).
[286] J. V. Wood, P. F. Mills, J. K. Bingham, and J. V. Bee, *Metall. Trans., A.* **10A,** 575 (1979).
[287] E. W. Müller and T. T. Tsong, *Prog. Surf. Sci.* **4,** 50 (1973).
[288] E. W. Müller, *J. Microsc. (Oxford)* **100,** 121 (1974).
[289] A. Van Oostrom, *CRC Crit. Rev. Solid State Sci.* **4,** 353 (1974).
[290] J. A. Panitz, *CRC Crit. Rev. Solid State Sci.* **5,** 153 (1975).
[291] E. W. Müller and S. V. Krishnaswamy, *in* "Characterization of Metal and Polymer Surfaces" (L.-H. Lee, ed.), Vol. 1, p. 21. Academic Press, New York, 1977.
[292] T. T. Tsong, *Chem Scr.* **14,** 7 (1979).
[293] A. R. Waugh and M. J. Southon, *Surf. Sci.* **89,** 718 (1979).
[294] P. A. Beaven, M. K. Miller, and G. D. W. Smith, *Inst. Metall. (London), Phase Transform* **2,** 1/12 (1979).

7.7. Field Desorption Microscopy

Both the field-electron and field-ion microscope provide nondestructive images of a tip surface by mapping local changes in its work function or the electric field distribution immediately above it. In principle, it is also possible to image the tip surface by desorbing a species from it. Müller[121] proposed to use barium for such a purpose as early as 1951, and later, with Bahadur,[128] he attempted to use nitrogen. The barium experiments were not reported in the literature, and the attempt to use nitrogen failed, probably because field-induced corrosion[126] was constantly changing the surface morphology of the tip.

Another imaging procedure was attempted by George[295] in 1965. He used a three-stage image intensifier in an attempt to record the field-evaporation process in vacuum. He hoped to record an image showing the position of atoms in the dissolving lattice. Inexplicably, no recognizable image was seen.

In 1972, Walko and Müller[152] repeated this experiment using a proximity-focused channel-plate image intensifier (with a gain of 10^6) located within the microscope chamber. They obtained both room-temperature and low-temperature images of field-evaporating tungsten. The images resembled their field-ion counterparts. Figure 22 shows a sequence of desorption images taken during field evaporation of tungsten at 80 K showing the gradual collapse of the (110) plane. At a tip bias of $V_0 = 11.415$ kV, the last atoms of the plane evaporate. In the next image, taken at 11.420 kV, underlying planes are imaged. At this point one atomic layer of the lattice [in the (110) region] has been removed.

If the individual desorption images of several net plane collapses are integrated, one would expect to obtain a contrastless image. Since the lattice atoms of each underlying layer do not necessarily occupy identical spatial positions, the image should "average out." Instead, the pattern is highly structured. These "multilayer images" were first observed by Waugh *et al.*[296] who found that they were characteristic of the material but not of its crystal structure. The cause of prominent features within a multilayer desorption image (such as shown in Fig. 23) is not completely understood. It is clear that the appearance of such features must be associated with the trajectories of the species being desorbed. Various explanations for image features involving ion-trajectory variations have appeared in the literature. These include directed surface migration immediately prior to desorption[297] and focusing by the polyhedral topography of the real tip surface.[298]

[295] T. H. George, *Bull. Am. Phys. Soc.* **10,** 493 (1965).
[296] A. R. Waugh, E. D. Boyes, and M. J. Southon, *Nature (London)* **253,** 342 (1975).
[297] A. R. Waugh, E. D. Boyes, and M. J. Southon, *Surf. Sci.* **61,** 109 (1976).
[298] S. V. Krishnaswamy, M. Martinka, and E. W. Müller, *Surf. Sci.* **64,** 23 (1977).

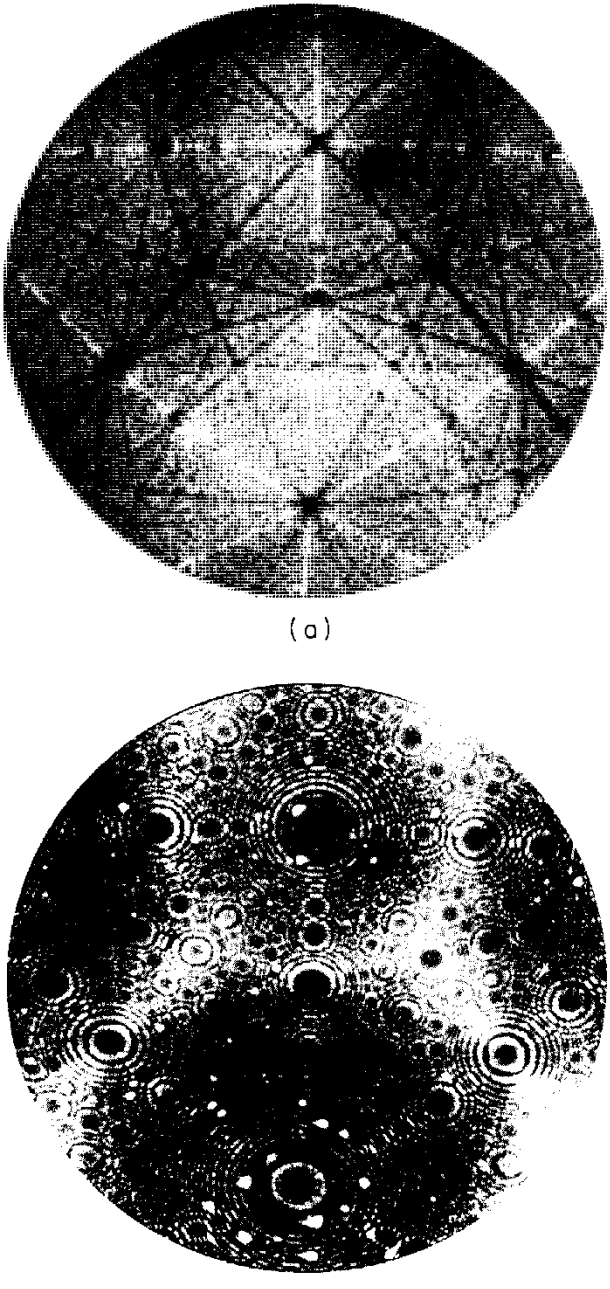

FIG. 23. (a) A multilayer desorption image of rhodium at 28 K in high vacuum. Approximately 30 atomic layers have been removed. (b) The corresponding helium-ion image is shown. (From Krishnaswamy *et al.*[298] Copyright North-Holland Physics Publishing, Amsterdam, 1977.)

7.7.1. The 10-cm Atom-Probe

Multilayer desorption images have raised a serious question about the reliability of atom-by-atom analysis in an atom-probe experiment. The atom-probe technique relies upon the assumption that a gas-phase species ionized above a surface atom during imaging and the desorbed surface atom itself will follow identical trajectories. Multilayer images show that the two trajectories can be quite different. This means that there can be a significant "aiming error" that can prevent an unambiguous identification of a species preselected in a field-ion image. The aiming problem was recognized as early as 1970. Tungsten atoms on the (110) plane could be detected only in the atom-probe if the probe hole was slightly shifted toward the center of the plane.[299]

In order to minimize the effect of the aiming error, the size of the probe hole can be increased. Because of the long draft distance in the TOF atom-probe, the probe hole can be eliminated and the entrance aperture of the detector used to define the region of the surface under examination.[300] By decreasing the length of the drift region, a large percentage of the surface can be examined. Panitz[146] showed that a drift region about ten centimeters in length would allow an appreciable portion of the tip to be examined with acceptable mass resolution. The resulting instrument was called a "10-cm" atom-probe.

7.7.2. The Imaging Atom-Probe

There are several advantages in examining a large area of the tip surface. A species having a small surface abundance produces a large easily identified mass peak, and species that do not survive field-ion imaging fields can be identified by recording a mass spectrum at their characteristic desorption field. These species can be imaged at the detector of the 10-cm atom-probe in order to deduce their distribution on the surface prior to desorption. The difficulty is that a desorption image cannot distinguish one desorbed species from another. Since several different species could desorb at one time, a unique crystallographic map of a preselected species is impossible to obtain.

An obvious solution to this problem is to activate the MCP detector of a desorption microscope at a fixed time after applying the high-voltage desorption pulse to the tip. By allowing the detector to have gain coincidentally with the arrival of a preselected species, only the preselected species will be imaged. Panitz,[301] developed a workable device based on this principle. It is

[299] S. S. Brenner and J. T. McKinney, *Surf. Sci.* **23**, 88 (1970).
[300] R. S. Chambers and G. Ehrlich, *J. Vac. Sci. Technol.* **13**, 273 (1976).
[301] J. A. Panitz, *J. Vac. Sci. Technol.* **11**, 206 (1974).

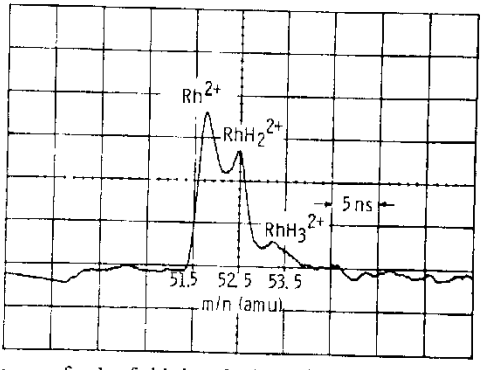

FIG. 24. Mass spectrum of pulse-field-desorbed rhodium in the presence of $\sim 8 \times 10^{-10}$ Torr of hydrogen. Because chemically stable hydrides of rhodium are unknown at zero field, it is assumed that rhodium hydride formation is favored in the high electric field generated at the tip surface. $V_{dc} = 7.1$ kV, $V_{pulse} \approx 1$ kV, $T \approx 80$ K. (From Panitz.[250])

known as the imaging atom-probe, or IAP. For the first time, the crystallographic distribution of a preselected surface species could be mapped over a large area of the tip surface. The mass resolution that can be achieved by the IAP is shown in Fig. 24. Since the mass resolution is ultimately limited by the energy spread of the desorbing ions, the imaging atom-probe will have a mass resolution as good as those of its counterparts that have much longer drift distances. All that is required is a correspondingly more accurate measurement of the shorter ion travel times. The imaging atom-probe has been used for metallurgical investigations,[302-309] surface studies,[305-307] as a tokamak diagnostic,[308-311] and for depth profiling of low-energy deuterium in tungsten.[310,311] A complete description of the experimental technique has been reviewed elsewhere.[250]

[302] A. R. Waugh, *J. Phys. E* **11**, 49 (1978).
[303] M. K. Miller, T. J. Godfrey, P. A. Beaven, P. R. Williams, K. M. Delargy, and G. D. W. Smith, *Ultramicroscopy* **4**, 383 (1979).
[304] A. R. Waugh, P. F. Mills, and M. J. Southon, *Philos. Trans. R. Soc. London Ser. A* **295**, 133 (1980).
[305] A. R. Waugh and M. J. Southon, *Surf. Sci.* **68**, 79 (1977).
[306] J. A. Panitz, *J. Vac. Sci. Technol.* **12**, 210 (1975).
[307] J. A. Panitz, *1979 DIE Workshop Hydrogen Met., Albuquerque* (available from NTIS, SAND79-0247C, 1979).
[308] G. L. Kellogg and J. A. Panitz, *J. Nucl. Mater.* **85**, 951 (1979).
[309] G. L. Kellogg and J. A. Panitz, *Appl. Surf. Sci.* **3**, 13 (1979).
[310] J. A. Panitz, *J. Vac. Sci. Technol.* **14**, 502 (1977).
[311] G. L. Kellogg, *Bull. Am. Phys. Soc.* **24**, 272 (1979).

7.8. Molecular Imaging with Ions

With the introduction of the low-temperature FIM in 1956, the resolution required to determine the tertiary structure of a biomolecule was available. Perhaps motivated by the success of the structure Watson and Crick[312] proposed for DNA, attempts to image biomolecules in the FIM began in the late 1960s. Two problems had to be considered. The first was to find a way to deposit a molecule of interest onto the apex of a tip. The second was to develop a scheme to ensure that the electric field strength required for field-ion imaging did not distort or destroy the adsorbed species. Of course, the act of removing a molecule from solution and drying it on the surface of a tip in high vacuum will probably distort the structure of the molecule. This problem is an inevitable consequence of any imaging technique that requires a high-vacuum environment.

In earlier field emission experiments, organic molecules were directly sublimed from the gas phase onto the surface of a tip cleaned by thermal annealing or field evaporation. Surface cleanliness was important because contrast in an FEEM image results from a local change in work function caused by an adsorbed molecule. It is not possible to determine from an FEEM image if a particular feature of interest is caused by the presence of the desired species or by an inadvertent contaminant. The organic molecules that were used in the FEEM experiments were very small, typically only five or ten lattice constants in extent. As a result, these species might be expected to be stearically constrained by substrate morphology. This means that surface morphology is important if it varies over distances comparable to the dimension of the molecule. On the other hand, most biological molecules are very large. They can easily span several hundred lattice constants. For these molecules, stearic effects should not be particularly important, and surface conditions could be much less critical. This is an important consideration because biological molecules cannot be sublimed in high vacuum onto a clean surface. They must be deposited from aqueous solution in the laboratory ambient.

Although many different deposition procedures were developed to place molecules on the surface of a tip,[98-100] their success could be evaluated only in terms of the FEEM and FIM images that they produced. An alternative approach to evaluate the success of deposition was introduced by Panitz and Giaever.[313] They used the transmission electron microscope (TEM) to observe thick protein layers formed on the tip surface by the immune reaction. It was found that a tip, when viewed in profile in the TEM, is an excellent substrate on which to observe thick protein layers. Because the tip scatters

[312] J. D. Watson and F. H. C. Crick, *Nature (London)* **171**, 737 (1953).
[313] J. A. Panitz and I. Giaever, *Surf. Sci.* **97**, 25 (1980).

electrons very effectively, it appears opaque in an electron micrograph. Although a single protein layer is barely detectable as a contrast variation along the tip contour, double and triple layers produced by the immune reaction are clearly visible. By correlating changes in the appearance of protein multilayers with corresponding changes in a dosing parameter, a simple aqueous deposition scheme was developed. By extending the TEM studies to a spherical protein molecule containing a core rich in iron, an aqueous dosing procedure for placing isolated molecules on a tip was subsequently developed.[314] Figure 25 shows the effectiveness of the technique by displaying a TEM micrograph of individual molecules of ferritin deposited on the contour of a large-radius tungsten tip. Ferritin is a nearly spherical molecule about 13 nm in diameter. It is a hollow shell assembled from twenty-four identical protein subunits. Its core contains about five thousand iron atoms incorporated in a complex ferric hydroxyphosphate polymer. Ferritin is found in the liver and spleen of higher organisms, where it acts as a reservoir for iron, an important but toxic element.

The electric field required for field-ion imaging is very large. Even if hydrogen is used as an imaging gas, the surface is subjected to a field of the order of 20 V nm^{-1}. Such fields produce a large outward-directed electrostatic stress that acts on all surface species, including the adsorbed molecules. It has the effect of tearing organic species apart and desorbing them from the tip surface. Abbott[315] used the FEEM to measure the average dc field strength required to desorb copper phthalocyanine, transfer RNA, and light meromyosin from a tip surface. He found values of 11.9, 10.3, and 7 V nm^{-1}, respectively. Melmed and Müller[106], using the FEEM, found that copper phthalocyanine was desorbed between 12.6 and 1.54 V nm^{-1}, depending on

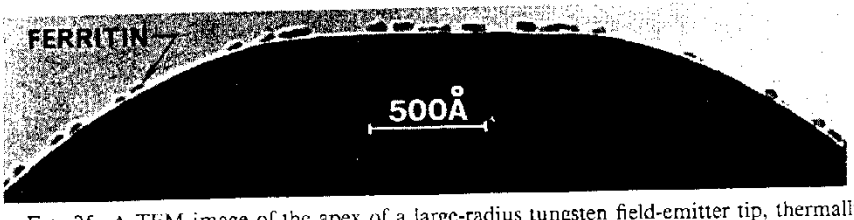

FIG. 25. A TEM image of the apex of a large-radius tungsten field-emitter tip, thermally annealed in high vacuum and covered with ferritin. Ferritin is a nearly spherical protein (~ 13 nm in diameter) that contains about 5000 iron atoms at its center. Only the iron-rich core of each ferritin molecule is visible in a TEM image. (After Panitz and Giaever.[314] Copyright North-Holland Physics Publishing, Amsterdam, 1981.)

[314] J. A. Panitz and I. Giaever, *Ultramicroscopy* **6**, 3 (1981).
[315] R. C. Abbott, *J. Chem. Phys.* **34**, 4533 (1965).

whether a quadruplet or doublet image was observed. More recently, Panitz[316] reported desorption field strengths for bovine serum albumine (BSA), BSA-antibody complexes, and ferritin. These species appear to be desorbed well below the best-image field for hydrogen.

In order to prevent a molecule from desorbing prior to field-ion imaging, Gurney *et al.*[317] proposed an ingenious imaging scheme. They suggested that one should embed a molecule on the tip surface within a thin deposit of a refractory metal. By increasing the electric field strength, the molecule might desorb from the surface, but it should leave a cavity in the deposited metal film. In principle, the shape of the cavity would be visible in a field-ion image and reflect the shape of the molecule prior to desorption. Graham *et al.*[318] tried to image molecules in this way but first annealed the layer in order to improve its uniformity. To improve image contrast, a series of helium field-ion images were taken at 20 K and superimposed. Each image was taken after one atomic layer had been removed by field evaporation. Several features suggestive of a molecular contour were obtained (Fig. 26), but reproducibility was poor.

Müller and Rendulic[319] used a variation of the shadow technique in an attempt to image vitamin B_{12} and coenzyme I (diphosphopyridine nucleotide). Their procedure involved incorporating the molecules in a polycrystalline platinum film, electrolytically deposited onto a tungsten tip. The deposited layer was alternately field-evaporated and imaged in helium in an attempt to expose and then observe randomly dispersed molecules. Single bright image spots and doublets were seen, but convincing images were not obtained. In particular, the expected fourfold symmetry of the vitamin B_{12} molecule was not seen.

In 1971, Machlin *et al.*[320] tried a novel method to image biological molecules. He hoped to observe the molecule in the process of desorbing. In his approach, a molecule-coated tip was placed in a field-ion microscope equipped with an image intensifier. The tip was cooled to about 5 K and imaged with hydrogen. The imaging procedure consisted of raising the dc tip voltage while recording the ion image on movie film. Machlin hoped to capture transient images that might appear before hydrogen BIV was reached. These images might reflect molecules or molecular fragments on the tip surface in the process of desorbing. A double blind procedure was used in an attempt to objectively evaluate the images. Many intriguing

[316] J. A. Panitz, *Bull. Am. Phys. Soc.* **24,** 272 (1979).
[317] T. Gurney, Jr., F. Hutchinson, and R. D. Young, *J. Chem. Phys.* **42,** 3939 (1965).
[318] W. R. Graham, R. Hutchinson, and D. A. Reed, *J. Appl. Phys.* **44,** 5155 (1973).
[319] E. W. Müller and K. D. Rendulic, *Science (Washington, D.C.)* **156,** 961 (1967).
[320] E. S. Machlin, A. Freilich, D. C. Agrawal, J. J. Burton, and C. L. Briant, *J. Microsc. (Oxford)* **104,** 127 (1975).

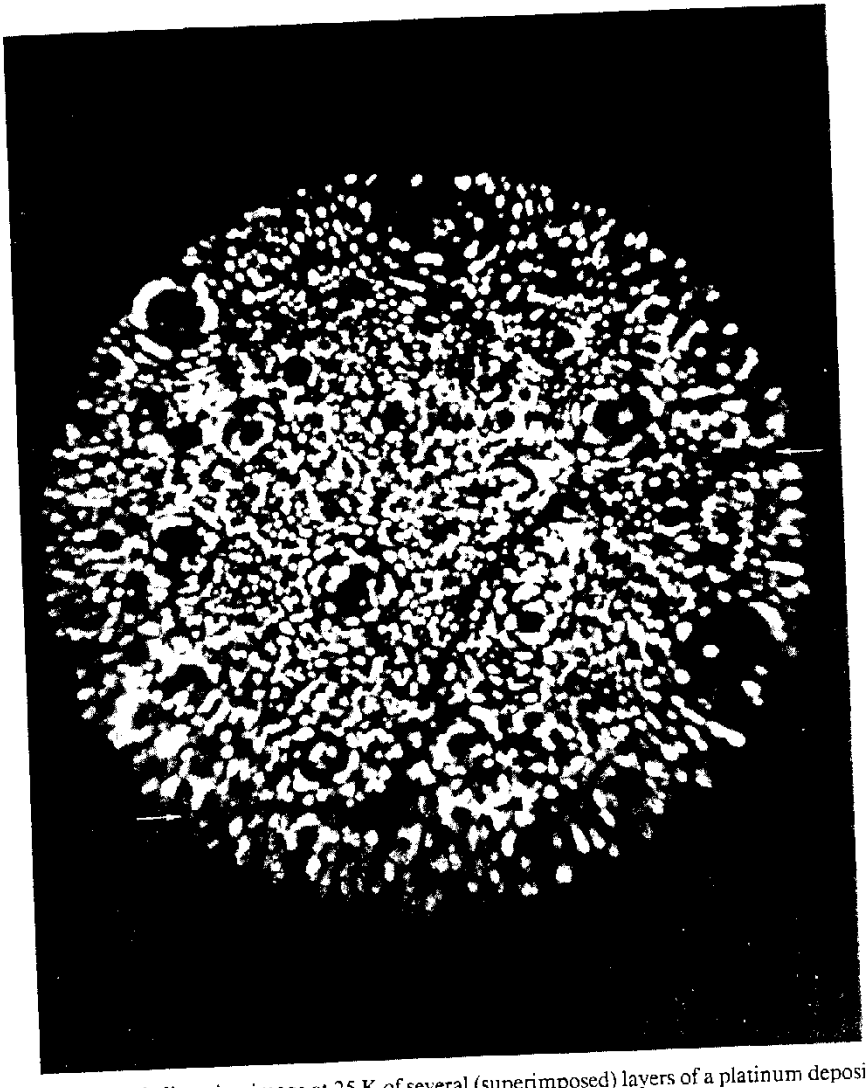

FIG. 26. A helium-ion image at 25 K of several (superimposed) layers of a platinum depositon an iridium tip. The tip was dipped into an aqueous solution of DNA (from micrococcus luteus) prior to platinum deposition in vacuum at 400 K. The dark feature indicated by arrows is thought to represent a DNA molecule. (From Graham *et al.*[318])

a
b
25 nm

features were seen (Fig. 27), but like all previous FIM imaging attempts, definitive images were never obtained.

In 1977 another imaging scheme was conceived.[321] Its virtue lies in its demonstrated ability to obtain reproducible nondestructive images of unstained biological molecules.[322-324] The technique is called field-ion tomography because it produces a series of contour slice (or "tomographic") images that show the distribution of molecules on a tip at various elevations above the tip surface. From these images, a three-dimensional reconstruction of the imaged species can be obtained.[325] The molecule of interest is deposited onto a field-emitter tip from aqueous solution.[314,326-327] After the tip is placed in a modified FIM, a thick layer of amorphous benzene ice is condensed from the gas phase onto the tip surface. Since the tip is cooled to a temperature below 30 K, the molecules of interest are effectively embedded within a frozen immobile matrix that completely surrounds and covers them. By increasing the tip voltage, the benzene layer can be controllably desorbed at a field strength below 4 V nm^{-1}. This means that the molecules of interest will not be removed during the imaging process.[323] Provided the benzene layer covers the deposited molecules, the benzene ion image at the detector will appear bright and relatively contrastless. However, as a molecule becomes exposed by the receding benzene layer, a dark region will appear in the image. Its contour will reflect the contour of the molecule defined by its intersection with the remaining benzene layer.

From a series of successive contour slice images taken during the removal of the benzene layer, a series of molecular contours are obtained. These can be digitally reconstructed in an objective way to produce a three-dimensional image of the molecular distribution on the surface that produced them.[325] An example of a field-ion tomographic image of ferritin is shown in Fig. 28. The image on the left is a field-ion tomographic image of unstained

FIG. 27. Transient images recorded during field-ion microscopy of an iridium tip on which a solution containing a single-stranded polynucleotide (poly-U) was freeze dried. The images were recorded using hydrogen as an imaging gas at a field strength of about (a) 5 V nm^{-1} and (b) 6.5 V nm^{-1}. The tip temperature was 5 K. (From Machlin *et al.*[320])

[321] J. A. Panitz and I. Giaever, *Abstr. 25th Int. Field-Emiss. Symp., Albuquerque, N.M., 1978*, published in *Ultramicroscopy* **4**, 366 (1979); *Abstr. 26th Field-Emiss. Symp., West Berlin, 1979*, published in *Ultramicroscopy* **5**, 248 (1980).

[322] J. A. Panitz, *J. Microsc. (Oxford)* **125**, 3 (1982).

[323] J. A. Panitz, *Ultramicroscopy* **7**, 241 (1982).

[324] J. A. Panitz and D. C. Ghiglia *J. Microsc. (Oxford)* **127**, 259 (1982).

[325] D. C. Ghiglia and M. Flickner, *Opt. Lett.* **7**, 116 (1982).

[326] J. A. Panitz, C. L. Andrews, and D. C. Beur, *JEMT* (1985). In press.

[327] J. A. Panitz, *Rev. Sci. Instrum.* (1985). In press.

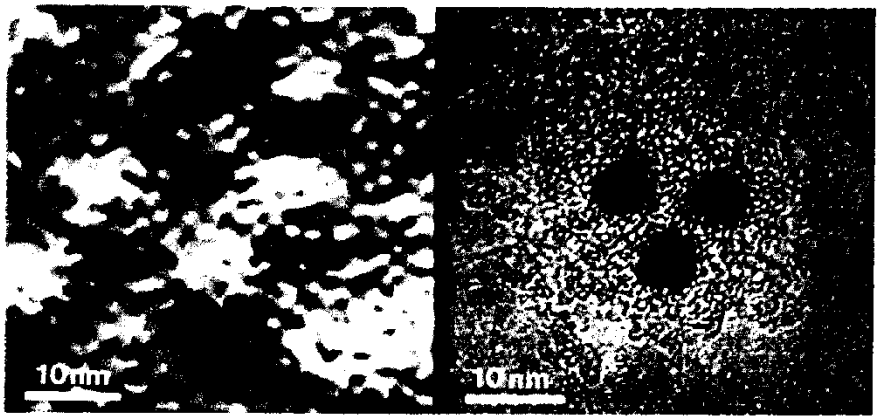

FIG. 28. Field-ion tomographic image of the unstained protein shell of several isolated ferritin molecules deposited onto the surface of a tungsten field-emitter tip (left). This image was digitally created from a series of contour slice images taken during controlled field desorption of a thick benzene layer condensed onto a molecule-coated tip at 20 K. The image at the right is a transmission electron micrograph of ferritin on a thin carbon substrate. Only the iron-rich cores of individual ferritin molecules can be seen. Their outer protein shell is invisible and is probably destroyed by electron bombardment during imaging. (From Panitz.[247] Copyright 1982 The Institute of Physics.)

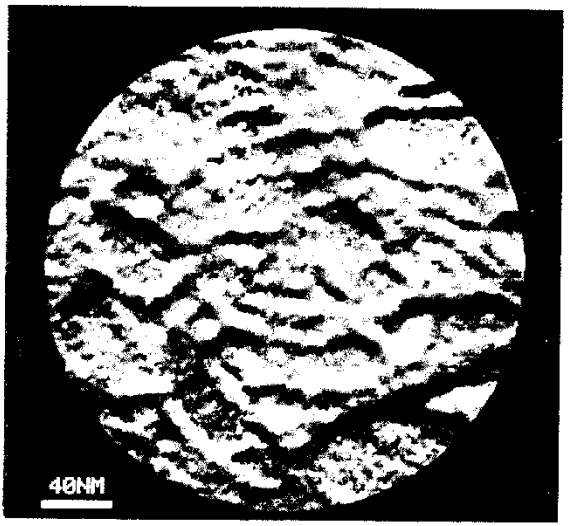

FIG. 29. A field-ion tomographic image of poly(GC) DNA on tungsten at 20 K.

ferritin molecules on a tungsten substrate.[324] The image on the right is a transmission electron micrograph of unstained ferritin on a thin carbon substrate. Unlike field-ion tomography, which provides a picture of the entire molecule, transmission electron microscopy can only provide an image of its iron-rich, electron-opaque core. An attempt to image DNA by field-ion tomography has recently been reported.[328] Figure 29 shows a tomographic image of DNA in which the characteristic stranded appearance of the molecule is evident. By combining field-ion tomography with the atom-probe techniques discussed previously, a real possibility exists for determining the molecular weight of a single, preselected macromolecule and visually mapping its constituent elements with a spatial resolution better than 1 nm.

Acknowledgments

The author gratefully acknowledges the United States Department of Energy, which has supported the author's research under Sandia Contract DE-AC04-76DP00789.

[328] J. A. Panitz, *Ultramicroscopy* **11**, 161 (1983).